

# 14

## Non-linear Oscillations and Chaos

The oscillations discussed in this book so far have all been restricted in amplitude to those which satisfy the equation of motion where the restoring force is a linear function of the displacement. This restriction was emphasized in Chapter 1 and from time to time its limiting influence has required further discussion; for example, in Chapter 6 on acoustic waves in a fluid. We now discuss some of the consequences when this restriction is lifted.

We begin with simple examples in mechanical, solid state and electrical oscillators. More complicated behaviour associated with chaos in these oscillators is also examined together with the appearance of chaos in biological and fluid mechanical systems.

### Free Vibrations of an Anharmonic Oscillator – Large Amplitude Motion of a Simple Pendulum

In Figure 1.1 the equation of motion of the simple pendulum was written in terms of its angular displacement as

$$\frac{d^2\theta}{dt^2} + \omega_0^2\theta = 0$$

where  $\omega_0^2 = g/l$ . Here, an approximation was made by writing  $\theta$  for  $\sin\theta$ ; the equation is valid for oscillation amplitudes within this limit. When  $\theta \geq 7^\circ$  however, this validity is lost and we must consider the more complicated equation

$$\frac{d^2\theta}{dt^2} + \omega_0^2 \sin\theta = 0$$

Multiplying this equation by  $2d\theta/dt$  and integrating with respect to  $t$  gives  $(d\theta/dt)^2 = 2\omega_0^2 \cos\theta + A$ , where  $A$  is the constant of integration. The velocity  $d\theta/dt$  is zero at the maximum angular displacement  $\theta = \theta_0$ , giving  $A = -2\omega_0^2 \cos\theta_0$  so that

$$\frac{d\theta}{dt} = \omega_0 [2(\cos\theta - \cos\theta_0)]^{1/2}$$

or, upon integrating,

$$\omega_0 t = \int \frac{d\theta}{\{2[\cos \theta - \cos \theta_0]\}^{1/2}}$$

If  $\theta = 0$  at time  $t = 0$  and  $T$  is the new period of oscillation, then  $\theta = \theta_0$  at  $t = T/4$ , and using half-angles we obtain

$$\omega_0 \frac{T}{4} = \int_0^{\theta_0} \frac{d\theta}{2[\sin^2 \theta_0/2 - \sin^2 \theta/2]^{1/2}}$$

If we now express  $\theta$  as a fraction of  $\theta_0$  by writing  $\sin \theta/2 = \sin(\theta_0/2) \sin \phi$ , where, of course,  $-1 < \sin \phi < 1$ , we have

$$\frac{1}{2}(\cos \theta/2)\delta\theta = (\sin \theta_0/2) \cos \phi \delta\phi$$

giving

$$\frac{\pi T}{2 T_0} = \int_0^{\pi/2} \frac{d\phi}{[1 - (\sin^2 \theta_0/2) \sin^2 \phi]^{1/2}}$$

where  $T_0 = 2\pi/\omega_0$ .

Expansion and integration gives

$$T = T_0(1 + \frac{1}{4} \sin^2 \theta_0/2 + \frac{9}{64} \sin^4 \theta_0/2 + \dots)$$

or approximately

$$T = T_0(1 + \frac{1}{4} \sin^2 \theta_0/2)$$

### (Problem 14.1)

## Forced Oscillations -- Non-linear Restoring Force

When an oscillating force is driving an undamped oscillator the equation of motion for such a system is given by

$$m\ddot{x} + s(x) = F_0 \cos \omega t$$

where  $s(x)$  is a non-linear function of  $x$ , which may be expressed in polynomial form:

$$s(x) = s_1 x + s_2 x^2 + s_3 x^3 \dots$$

where the coefficients are constant. In many practical examples  $s(x) = s_1 x + s_3 x^3$ , where the cubic term ensures that the restoring force  $s(x)$  has the same value for positive and negative displacements, so that the vibrations are symmetric about  $x = 0$ . When  $s_1$  and  $s_3$  are both positive the restoring force for a given displacement is greater than in the linear case and, if supplied by a spring, this case defines the spring as 'hard'. If  $s_3$  is negative the

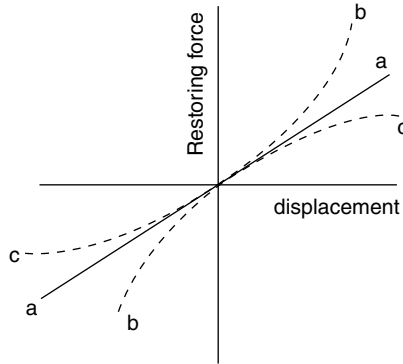


**Figure 14.1** Oscillator displacement versus restoring force for (a) linear restoring force, (b) non-linear 'hard' spring, and (c) non-linear 'soft' spring

restoring force is less than in the linear case and the spring is 'soft'. In Figure 14.1 the variation of restoring force is shown with displacement for  $s_3$  zero (linear),  $s_3$  positive (hard) and  $s_3$  negative (soft). We see therefore that the large amplitude vibrations of the pendulum of the previous section are soft-spring controlled because

$$\sin \theta \approx \theta - \frac{1}{3}\theta^3$$

Figure 14.2 shows a mass  $m$  attached to points D and D', a vertical distance  $2a$  apart, by two light elastic strings of constant stiffness  $s$  and subjected to a horizontal driving force  $F_0 \cos \omega t$ . At zero displacement the tension in the strings is  $T_0$  and at a displacement  $x$  (not limited in value) the tension is  $T = T_0 + s(L - a)$  where  $L$  is the stretched string length.

The equation of motion (neglecting gravity) is

$$\begin{aligned} m\ddot{x} &= -2T \sin \theta + F_0 \cos \omega t \\ &= -2[T_0 + s(L - a)] \frac{x}{L} + F_0 \cos \omega t \end{aligned}$$

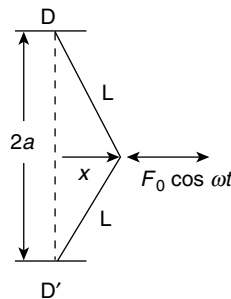


**Figure 14.2** A mass  $m$  supported by elastic strings between two points D and D' vertically separated by a distance  $2a$  and subjected to a lateral force  $F_0 \cos \omega t$

Inserting the value

$$L = a \left[ 1 + \left( \frac{x}{a} \right)^2 \right]^{1/2}$$

and expanding this expression in powers of  $x/a$ , we obtain by neglecting terms smaller than  $(x/a)^3$

$$m\ddot{x} = -\frac{2T_0}{a}x - \frac{(sa - T_0)}{a^3}x^3 + F_0 \cos \omega t$$

which we may write

$$\ddot{x} + s_1x + s_3x^3 = \frac{F_0}{m} \cos \omega t$$

where

$$s_1 = \frac{2T_0}{ma} \quad \text{and} \quad s_3 = \frac{sa - T_0}{ma^3}$$

If  $s_3$  is small we assume (as a first approximation) the solution  $x_1 = A \cos \omega t$ , which yields from the equation of motion

$$\ddot{x}_1 = -s_1A \cos \omega t - s_3A^3 \cos^3 \omega t + \frac{F_0}{m} \cos \omega t$$

Since  $\cos^3 \omega t = \frac{3}{4} \cos \omega t + \frac{1}{4} \cos 3\omega t$ , this becomes

$$\ddot{x}_1 = -(s_1A + \frac{3}{4}s_3A^3 - F_0/m) \cos \omega t - \frac{1}{4}s_3A^3 \cos 3\omega t$$

Integrating twice, where the constants become zero from initial boundary conditions, gives as a second approximation to the equation

$$\ddot{x} + s_1x + s_3x^3 = \frac{F_0}{m} \cos \omega t$$

the solution

$$x_2 = \frac{1}{\omega^2} \left( s_1A + \frac{3}{4}s_3A^3 - \frac{F_0}{m} \right) \cos \omega t + \frac{s_3A^3}{36\omega^2} \cos 3\omega t$$

Thus, for  $s_3$  small we have a value of  $\omega$  appropriate to a given amplitude  $A$ , and we can plot a graph of amplitude versus driving frequency. Note that we have a third harmonic. We see that for a system with a non-linear restoring force resonance does not exist in the same way as in the linear case. In the example above, even when no damping is present, the amplitude will not increase without limit for a driving force of a given frequency, for if  $\omega$  is the natural frequency at low amplitude it is no longer the natural frequency at high amplitude. For  $s_3$  positive (hard spring) the natural frequency increases with increasing amplitude and the

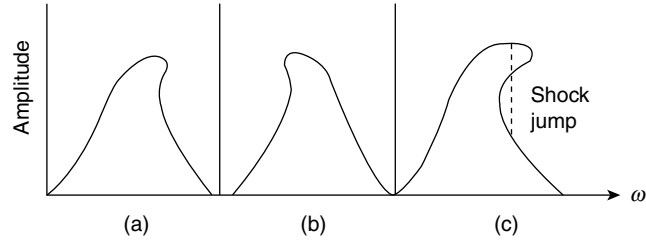


**Figure 14.3** Response curves of amplitude versus frequency for oscillators having (a) a 'hard' spring restoring force, and (b) a 'soft' spring restoring force. In the extreme case (c) the tilt of the maximum is sufficient to allow multi-valued amplitudes at a given frequency and 'shock jumps' may occur (See Figure 15.1 for comparable behaviour in a high amplitude sound wave.)

amplitude versus frequency curve has a tilted maximum (Figure 14.3a). For a soft spring,  $s_3$  is negative and the behaviour follows Figure 14.3b. It is possible for the tilt to become so pronounced (Figure 14.3c) that the amplitude is not single valued for a given  $\omega$  and shock jumps in amplitude may occur at a given frequency (see the next chapter on the development of a shock front in a high amplitude acoustic wave).

**(Problems 14.2, 14.3)**

## Thermal Expansion of a Crystal

Chapter 1 showed that the curve of potential energy versus displacement for a linear oscillator was parabolic. Small departures from this curve are consistent with anharmonic oscillations. Consider the potential energy curve for a pair of neighbouring ions of opposite charge  $\pm e$  in a crystal lattice such as that of KCl. If  $r$  is the separation of the ions the mutual potential energy is given by

$$V(r) = \frac{\alpha e^2}{r} + \frac{\beta}{r^p}$$

where  $\alpha$  and  $\beta$  are positive constants and  $p = 9$ . This is plotted in Figure 14.4, which shows that the potential energy curve is no longer parabolic. The first term of  $V(r)$  is the energy due to Coulomb attraction; the second is that of a repulsive force. The value of  $\alpha$  depends upon the presence of neighbouring ions and is about 0.3. The constant  $\beta$  can be found in terms of  $\alpha$  and the equilibrium separation  $r_0$  because, in equilibrium,

$$\left(\frac{dV}{dr}\right)_{r=r_0} = \frac{\alpha e^2}{r_0^2} - \frac{p\beta}{r_0^{p+1}} = 0$$

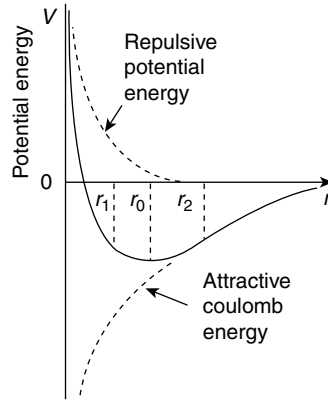


**Figure 14.4** Non-parabolic curve of mutual potential energy between oppositely charged ions in the lattice of an ionic crystal (NaCl or KCl). The combination of repulsive and attractive forces yields an equilibrium separation  $r_0$ . Very small energy increments give harmonic motion about  $r_0$  but oscillations at higher energies are anharmonic, leading to thermal expansion of the crystal

giving

$$\beta = \frac{\alpha e^2 r_0^{p-1}}{p}$$

X-ray diffraction from such crystals gives  $r_0 = 3.12 \text{ \AA}$  for KCl, so that  $\beta$  may be found numerically.

To consider small displacements from the equilibrium value  $r_0$  let us expand  $V(r)$  about  $r = r_0$  in a Taylor series to give

$$V(r) = V(r_0) + x \left( \frac{dV}{dr} \right)_{r_0} + \frac{x^2}{2!} \left( \frac{d^2V}{dr^2} \right)_{r_0} + \frac{x^3}{3!} \left( \frac{d^3V}{dr^3} \right)_{r_0}$$

where  $x = r - r_0$ . Since  $(dV/dr)_{r_0} = 0$ , we may write

$$V(r) - V(r_0) = V(x) = A \frac{x^2}{2!} + \frac{Bx^3}{3!}$$

The quantity  $Ax^2/2$  is the quadratic term familiar in the linear oscillator, so that for very small disturbances the bottom of the potential energy curve is parabolic, and a small gain in energy causes the ion pair to oscillate symmetrically about  $r = r_0$ . An increase in the ion pair energy involves the second term  $Bx^3/6$ , and oscillations are no longer symmetric about  $r_0$ , because  $|r_2 - r_0| > |r_1 - r_0|$  in Figure 14.4. Hence the time average for  $r - r_0$  is not zero as it is for a linear oscillator, and this time average  $r_t > r_0$ . If all ion pairs acquire this amount of energy, for example by heating, the crystal expands. We may consider the force between the two ions as

$$F = -\frac{dV}{dx} = -Ax - \frac{Bx^2}{2}$$

and note that the quadratic term here is responsible for the lack of symmetry in the motion. If it were a cubic term as in the previous example the symmetry of motion about  $r_0$  would still occur. The coefficient  $A$  in the force equation is the force constant in the discussion on crystals in Chapters 5 and 6 and leads directly to Young's modulus. The coefficient  $B$  gives information on the coefficient of thermal expansion of the crystal.

**(Problems 14.4, 14.5)**

## Non-linear Effects in Electrical Devices

A feature of the non-linearity in the mechanical devices discussed earlier was the introduction of harmonics of the fundamental frequency of the driving force. It is comparatively simple to avoid these effects of non-linearity in electronic systems by choosing a small linear portion of the operating characteristic and amplifying the response in stages. In an electromechanical device such as a piezoelectric crystal linearity is again achieved by restricting all oscillations to small amplitudes and amplifying the response. In electroacoustic devices such as microphones and loudspeakers the introduction of harmonics often leads to severe distortion. In the loudspeaker of Figure 14.5 even if a pure sinusoidal wave is delivered to the speech coil it is difficult to provide a mechanical suspension for the cone which has a linear response. The cone acts as a piston radiating acoustic power, and limitation of amplitude together with inevitable mismatching of acoustic impedances reduces the efficiency of transforming electrical into acoustic power to less than 10%. Fortunately the ear is a sensitive device.

Non-linear electrical oscillators are, however, often used, and Figure 14.6a shows a 'relaxation oscillator' circuit where a capacitance is discharged very rapidly through a gaseous conductor such as a hydrogen tube.  $E$  is the constant charging potential and  $i$  is the instantaneous value of the current which charges the capacitor through the resistor  $R$  to a potential  $V_s$ , the striking potential, at which the gas in the tube is ionized. The tube

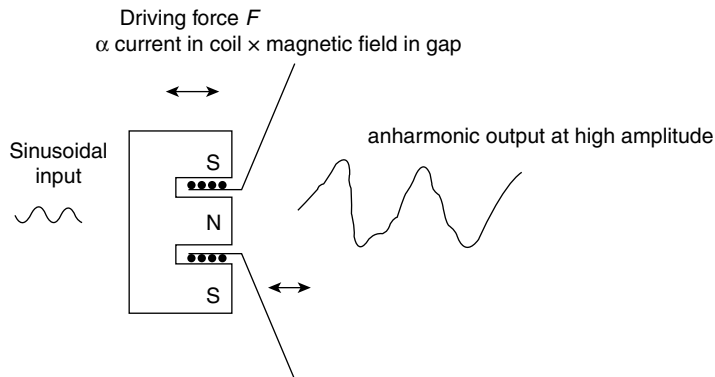


**Figure 14.5** A pure sinusoidal wave input to an electroacoustical device such as a loudspeaker will lead to distorted sound output if the cone suspension has a non-linear stiffness at high amplitudes

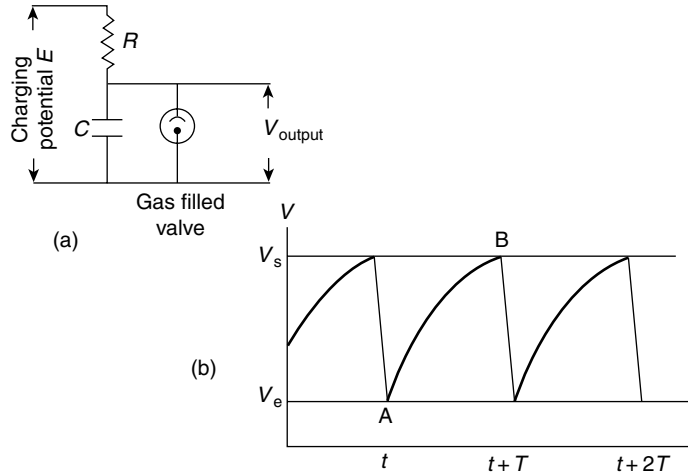


**Figure 14.6** Electrical circuit of a non-linear 'relaxation oscillator'. A capacitance  $C$  is charged through a resistance  $R$  to a potential  $V_s < E$ , at which the gas-filled valve strikes and rapidly discharges the condenser to an extinction potential  $V_e$ , when the valve ceases to conduct and the cycle is repeated

becomes highly conducting and discharges the capacitance in a negligibly short time to  $V_e$ , the extinction potential, at which the tube ceases to conduct. The capacitance charges again to  $V_s$  and the cycle is repeated. The variation of voltage across the capacitance with time is shown in Figure 14.6b. Assume that at point A and time  $t$  the capacitance has just discharged. If current  $i_0$  is flowing at time  $t = 0$  then

$$V_e = E - i_0 R e^{-t/RC}$$

The capacitance charges to the potential  $V_s$  in a time  $\tau$  so that

$$V_s = E - i_0 R e^{-(t+\tau)/RC}$$

giving

$$\begin{aligned} V_s - V_e &= i_0 R (e^{-t/RC} - e^{-(t+\tau)/RC}) \\ &= i_0 R e^{-t/RC} [1 - e^{-\tau/RC}] \\ &= (E - V_e) [1 - e^{-\tau/RC}] \end{aligned}$$

giving

$$e^{-\tau/RC} = \frac{E - V_s}{E - V_e}$$

or

$$\tau = RC \left[ \log_e \left( \frac{E - V_e}{E - V_s} \right) \right]$$

The period of oscillation is therefore directly proportional to the charging time constant  $RC$ .

A more sophisticated circuit produces a linear charging system with a very short discharge time so that the exponential voltage output becomes linear and gives a 'sawtooth' waveform. From Chapter 10 we know that this periodic function contains many harmonics. A sawtooth voltage output applied to the time base of an oscilloscope produces a linear sweep of the spot across the tube.

## Electrical Relaxation Oscillators

Van der Pol and Chaos (1926–1927)

The work of Van der Pol continues to attract the attention of research workers in chaos chiefly because of an equation he derived at that time. His relaxation oscillator was a multivibrator, a two stage resistance-capacity coupled amplifier with the output of the second triode fed back as input to the grid of the first. His analysis used the mechanical form of the damped simple harmonic equation with a negative resistance term which increased the amplitude, thus

$$\ddot{x} - \alpha x + \omega^2 x = 0$$

with a solution

$$x = C e^{+\alpha t/2} \sin [(\omega^2 - \alpha^2/4)t + \phi]$$

for  $\alpha > 0$  and  $\alpha^2/4 < \omega^2$ .

He restricted the unlimited growth of  $x$  by replacing  $\alpha$  with  $\alpha - 3\gamma/x^2$  where  $\gamma$  is a constant, writing  $\omega t = t'$  and  $x = (\alpha/3\gamma)^{1/2} v$  to give his equation the form

$$\ddot{v} - \varepsilon(1 - v^2)\dot{v} + v = 0$$

where  $\varepsilon = \alpha/\omega$  and  $\dot{v} = dv/dt'$ .

It is this equation with a forcing term  $A \sin \omega_0 t$  on the right hand side which is known as Van der Pol's equation and which has formed the basis of a number of studies in chaos, one of which we shall meet later. Van der Pol found that as  $\varepsilon$  increased his oscillator gradually assumed the period  $\tau = RC$  with the output for  $\varepsilon = 10$  shown in Figure 14.7 (Van der Pol, 1926).

Even more interesting from the viewpoint of chaos was the oscillator by which he could produce subharmonics of its natural frequency. Such a phenomenon, period doubling, tripling, etc. is now recognized as an early sign of chaos, indeed Li and Yorke (1975) have published a paper entitled 'Period 3 implies Chaos'.

Van der Pol's period doubling circuit is shown in Figure 14.8. With  $E_0 = 0$  and  $C = 10^{-3} \mu\text{F}$  the relaxation frequency of the system was  $10^3$  cycles. Setting  $E_0 \sin \omega t$  at  $7.5 \sin 2\pi 10^3 t$  he was able, by increasing  $C$  through the range  $5-40 \times 10^{-3} \mu\text{F}$  to produce subharmonics  $\omega/2, \omega/3 \dots \omega/40 \dots \omega/200$ . He registered the output on a pair of loosely coupled telephone earpieces and his paper makes the interesting comment that 'often an irregular noise is heard in the telephone receivers before the frequency jumps, however this is a subsidiary phenomenon'. In fact, such *internally* generated noise accompanied by subharmonics is one of the early signs of chaos (Van der Pol and Van der Mark, 1927).

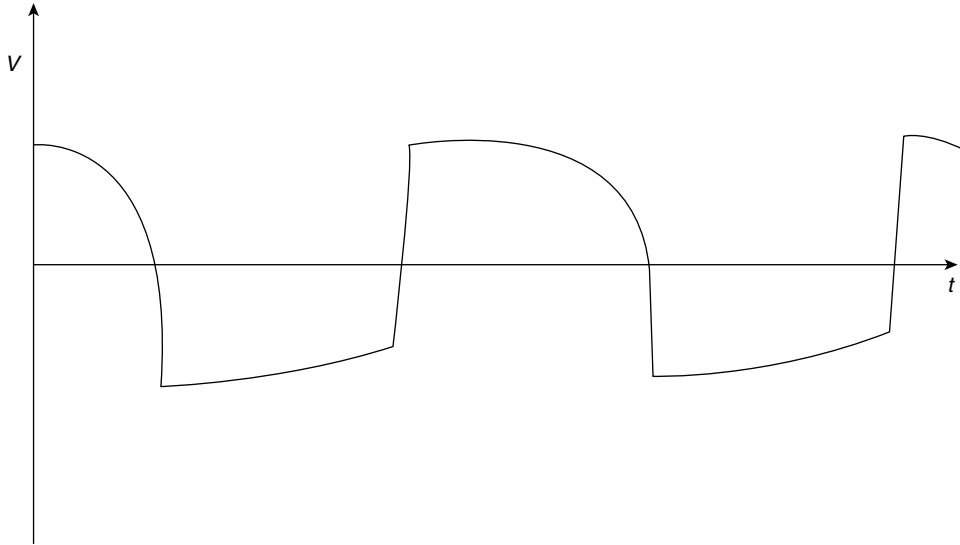


**Figure 14.7** Non-linear relaxation oscillations of period  $\tau = RC$  for an unforced Van der Pol system

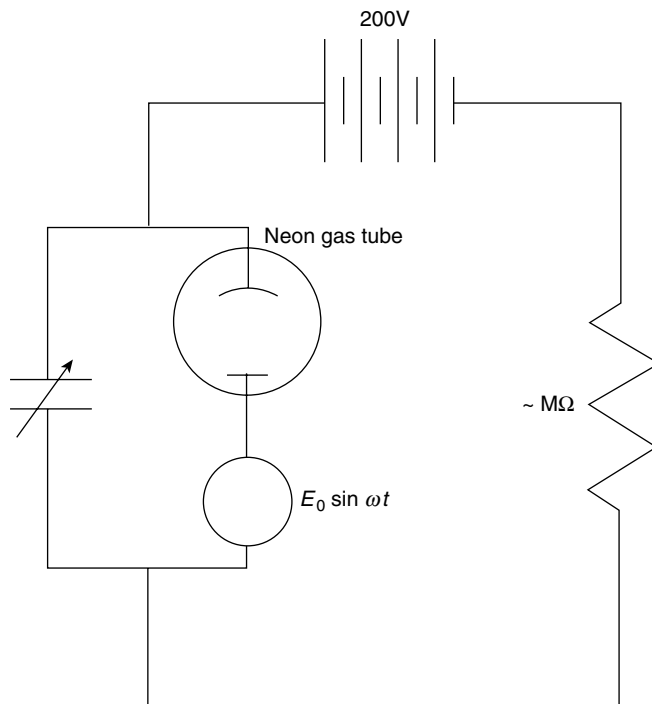


**Figure 14.8** Van der Pol's period doubling circuit

## Chaos in Population Biology

Chronological accounts of a modern research topic rarely present the most coherent picture. The significance of early developments is not always recognized until much later; indeed the first recorded strange or chaotic attractor, that of Lorenz in 1963, comes at the end of this account but only because of its level of sophistication. Even the simple example with which we begin was not fully explained when it first appeared.

Despite its simplicity the example of population biology reveals many of the characteristics displayed by chaotic systems. These are:

- The chaos is deterministic and not random; that is, the paths followed by trajectories are governed by solutions to given non-linear equations.
- Trajectories from closely neighbouring starting points diverge with time.
- Trajectories can, according to the conditions, finish on a stable point attractor, they can diverge to infinity from a repeller or at some stage they can orbit in what is known as a limit cycle.
- Such a limit cycle can develop an infinite series of period doubling; odd number periods may be generated, also completely aperiodic trajectories which still remain within a bounded region of space.
- With the appearance of chaotic motion the sharp definition of these frequencies is gradually overcome by a growing background of wide band noise which is *internally* generated.

A number of equations dealing with population biology has been widely studied but we consider the simplest, a quadratic equation discussed by May (1976) in a classic review.

This is known as the logistic map and is given by

$$x_{n+1} = 4\lambda x_n(1 - x_n)$$

where the subscripts refer to the year in which the population was measured and  $\lambda$  is a parameter. Restricting the values of  $x$  and  $\lambda$  to  $0 < x < 1$  and  $0 < \lambda < 1$  is a scaling device which keeps the dynamics within the limits of a diagram. Because it involves only the coordinate  $x$  this logistic equation is known as a one-dimensional map.

Much of the behaviour of populations under this quadratic rule is shown by the interaction of the parabola and the straight line bisector  $x_{n+1} = x_n$  of gradient unity and this behaviour is divided into three distinct categories by the  $\lambda$  ranges  $0 < \lambda < \frac{1}{4}$ ,  $\frac{1}{4} < \lambda < \frac{3}{4}$  and  $\frac{3}{4} < \lambda < 1$ .

To illustrate the general use of the bisector consider what happens to a population with a constant reproduction rate; that is, the straight line  $x_{n+1} = 4\lambda x_n$ . Figure 14.9a shows the line for  $\lambda > \frac{1}{4}$  compared with the bisector  $x_{n+1} = x_n$ . Taking  $x_0$  as the starting value of the population gives  $x_1$  on the  $\lambda > \frac{1}{4}$  line which then projects horizontally to the same value ( $x_1$ ) on the bisector. This gives the value  $x_1$  on the base line which projects vertically to the  $\lambda > \frac{1}{4}$  line to give  $x_2$  and the process is repeated. Evidently for  $\lambda > \frac{1}{4}$  the population

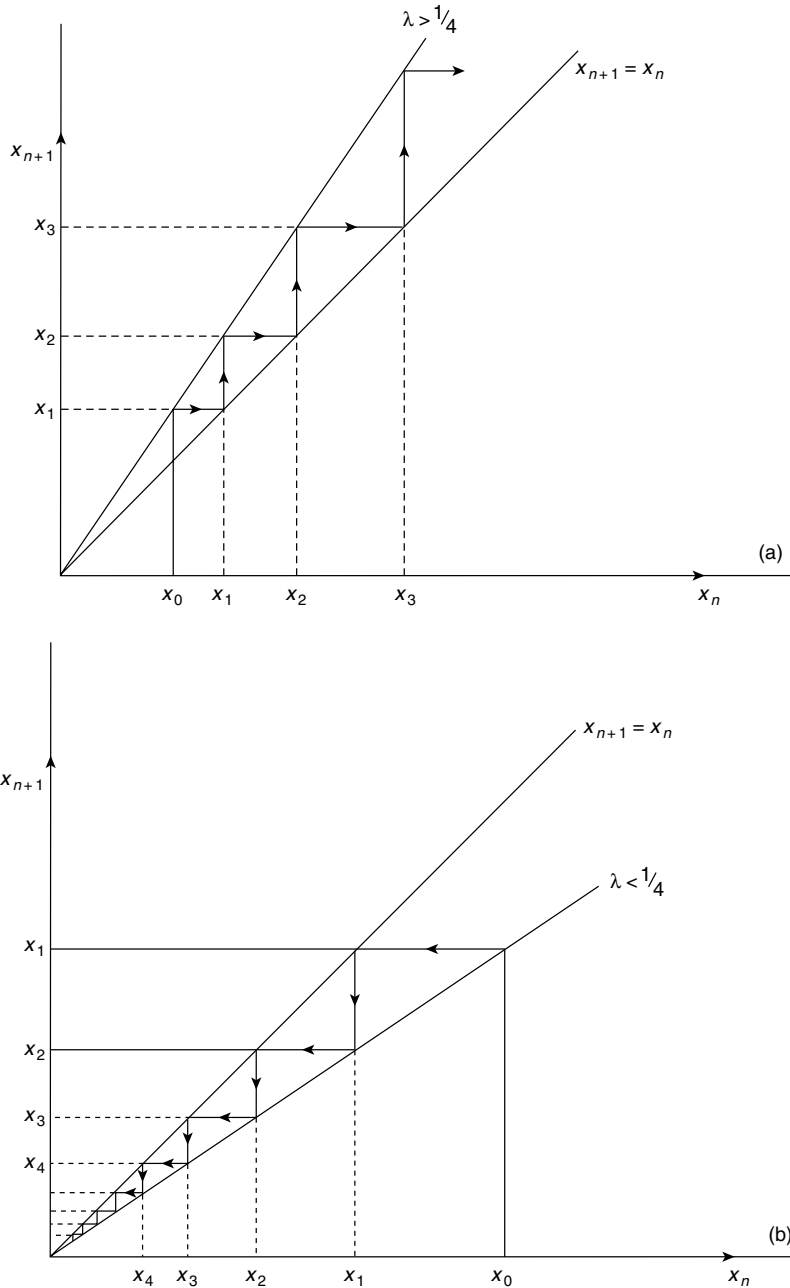


**Figure 14.9** Change of population with constant reproduction rate given by  $x_{n+1} = 4\lambda x_n$ . (a) for  $\lambda > \frac{1}{4}$  the population  $\rightarrow \infty$  as the trajectories move away from the origin (a repeller). (b) For  $\lambda < \frac{1}{4}$  the population is extinguished, all trajectories moving to the stable point attractor at zero. The initial population at  $x_0$  gives  $x_1$  on the  $\lambda > \frac{1}{4}$  line which projects horizontally to the same value on the bisector  $x_{n+1} = x_n$ . The value  $x_1$  projects vertically to  $x_2$  on the  $\lambda > \frac{1}{4}$  line and the process repeats itself. Similarly for  $\lambda < \frac{1}{4}$

increases without limit, the trajectories move to infinity from a repellor. For  $x < \frac{1}{4}$ , Figure 14.9b, the same process of horizontal and vertical projection produces  $x_1 < x_0$  and the population is extinguished, all trajectories moving to the stable point attractor at zero.

The method is equally applicable to the parabola

$$x_{n+1} = 4\lambda x_n(1 - x_n)$$

For  $\lambda > \frac{1}{4}$  we have Figure 14.10 and where the curve and the bisector intersect we have  $x_{n+1} = x_n$  corresponding to a fixed point in the iteration process. Writing this value as  $x_{n+1} = x_n = x^*$  we find from  $x^* = 4\lambda x^*(1 - x^*)$  the two roots  $x^* = 0$  and  $x^* = 1 - \frac{1}{4\lambda}$  each of which is a fixed point.

Restricting  $x$  and  $\lambda$  to the values between 0 and 1 gives for  $\lambda < \frac{1}{4}$  only the value  $x^* = 0$  but for  $\frac{1}{4} < \lambda < 1$ ,  $x^*$  may take both values. If  $x^*$  is stable; that is, a fixed point to which the end points of all trajectories become infinitely close, Figure 14.10, it is a point attractor and this stability depends on the slope of the curve at  $x^*$ . We write  $x_{n+1} = 4\lambda x_n(1 - x_n) = f(x_n)$  and if  $-1 < f'(x) < 1$  at  $x^*$ ,  $x^*$  is stable. When the slope  $f'(x)$  equals  $-1$  stability is lost and  $x^*$  bifurcates into two new values, each of which is stable. This is called a pitchfork bifurcation and is the origin of the period doubling sequence in the logistic map. Odd numbered periodic cycles arise at a later stage from bifurcations into pairs of new values, only one of each pair being stable. These are called tangent bifurcations.

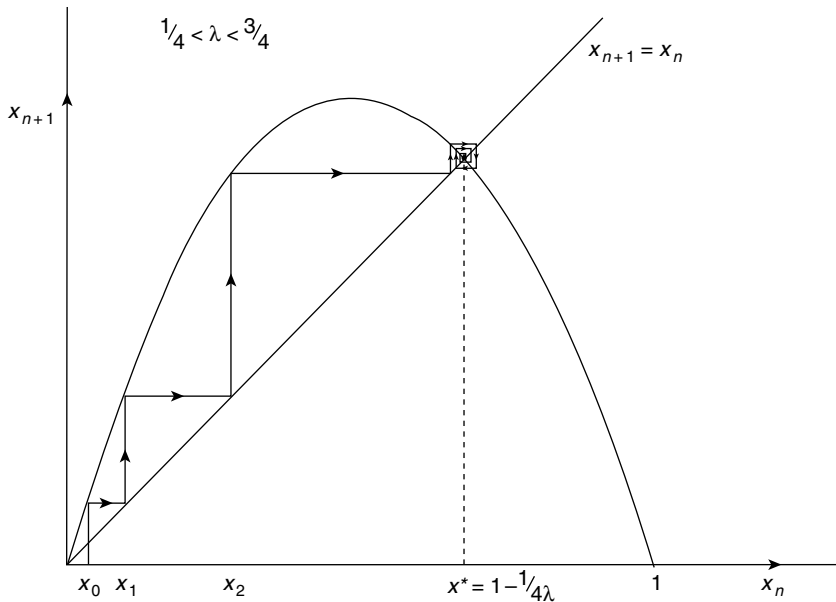


**Figure 14.10** The logistic equation  $x_{n+1} = 4\lambda x_n(1 - x_n)$  cut by the bisector  $x_{n+1} = x_n$  at the points  $x^* = 0$  and  $x^* = 1 - \frac{1}{4\lambda}$ . When  $\frac{1}{4} < \lambda < \frac{3}{4}$  the latter value of  $x^*$  is a stable point attractor for all trajectories as shown

The dependence of stability upon  $f'(x)$  at the fixed point  $x^*$  follows from Taylor's theorem for, with  $x_{n+1} = f(x_n)$  and  $x_n = x^* + \varepsilon_n$  where  $\varepsilon_n$  is a very small quantity, we have

$$\begin{aligned}x_{n+1} &= f(x^* + \varepsilon_n) \approx f(x^*) + \varepsilon_n f'(x^*) \\ &= x^* + \varepsilon_n f'(x^*)\end{aligned}$$

because  $x^* = f(x^*)$  at this fixed point  $x^*$ .

Now  $x_{n+1} = x^* + \varepsilon_{n+1}$ , giving  $f'(x^*) = \varepsilon_{n+1}/\varepsilon_n$  and for  $n \rightarrow \infty$ ,  $\varepsilon_{n+1} \rightarrow 0$  only if  $-1 < f'(x) < 1$ .

Thus,  $x^* = 0$  is a stable point attractor for all trajectories when  $\lambda < \frac{1}{4}$  but becomes unstable at  $\lambda = \frac{1}{4}$  while  $x^* = 1 - \frac{1}{4\lambda}$  is a stable point attractor for all trajectories when  $\frac{1}{4} < \lambda < \frac{3}{4}$ . At  $\lambda = \frac{3}{4}$  the slope of  $f(x)$  at  $x^* = 1 - \frac{1}{4\lambda}$  equals  $-1$ , stability is lost,  $x^*$  bifurcates and a stable oscillation between two new values  $x_1^*$  and  $x_2^*$  develops. We can see this by studying the behaviour of  $x_{n+2}$  versus  $x_n$ , obtained by a double application of the logistic equation.

We can express  $x_{n+2} = f(x_{n+1}) = ff(x_n) = f^2(x_n)$  where the superscript defines the double application. A graph of  $f^2(x)$ , which is symmetric, is shown in Figure 14.11a where the central minimum decreases as  $\lambda$  increases. The bisector is now of course  $x_{n+2} = x_n$  and, as shown, it cuts  $f^2(x)$  at three fixed points. The value of  $\lambda$  is chosen so that  $x_1^*$  is near the minimum and  $x_2^*$  is near a maximum. The slope of  $f^2(x)$  (written  $f^{2'}(x)$ ) at  $x_1^*$  and  $x_2^*$  is therefore close to zero and  $x_1^*$  and  $x_2^*$  are stable fixed points of  $f^2(x)$ . It is at this value of  $\lambda = \frac{3}{4}$  that period doubling begins.

The third fixed point  $x^*$  is clearly the original fixed point of  $f(x)$ . This follows from noting that the point  $x^* = x_n = x_{n+1} = x_{n+2}$  falls on both  $f(x)$  and  $f^2(x)$  and on their respective bisectors. In addition, the stability behaviour of  $x^*$  is the same for  $f(x)$  and  $f^2(x)$ . We can show this via the chain rule, for if

$$x_2 = f(x_1) = f^2(x_0) \quad \text{where} \quad x_1 = f(x_0)$$

then

$$f^{2'}(x) = f'(x_1) = \frac{d[f(x_1)]}{dx_1} \frac{dx_1}{dx} = \left[ \frac{df(x_1)}{dx_1} \right] f'(x)$$

where all derivatives are evaluated at  $x = x_0$ . This result holds for higher values of the superscript  $n$  in  $f^n(x)$ .

Taking  $x_0$  as the fixed point  $x^*$  then

$$x^* = x_0 = x_1 = x_2$$

and

$$f^{2'}(x^*) = f'(x^*)f'(x^*) = (f'(x^*))^2.$$

Thus, if  $x^*$  is stable (unstable) in  $f(x)$  then it is stable (unstable) in  $f^2(x)$ .

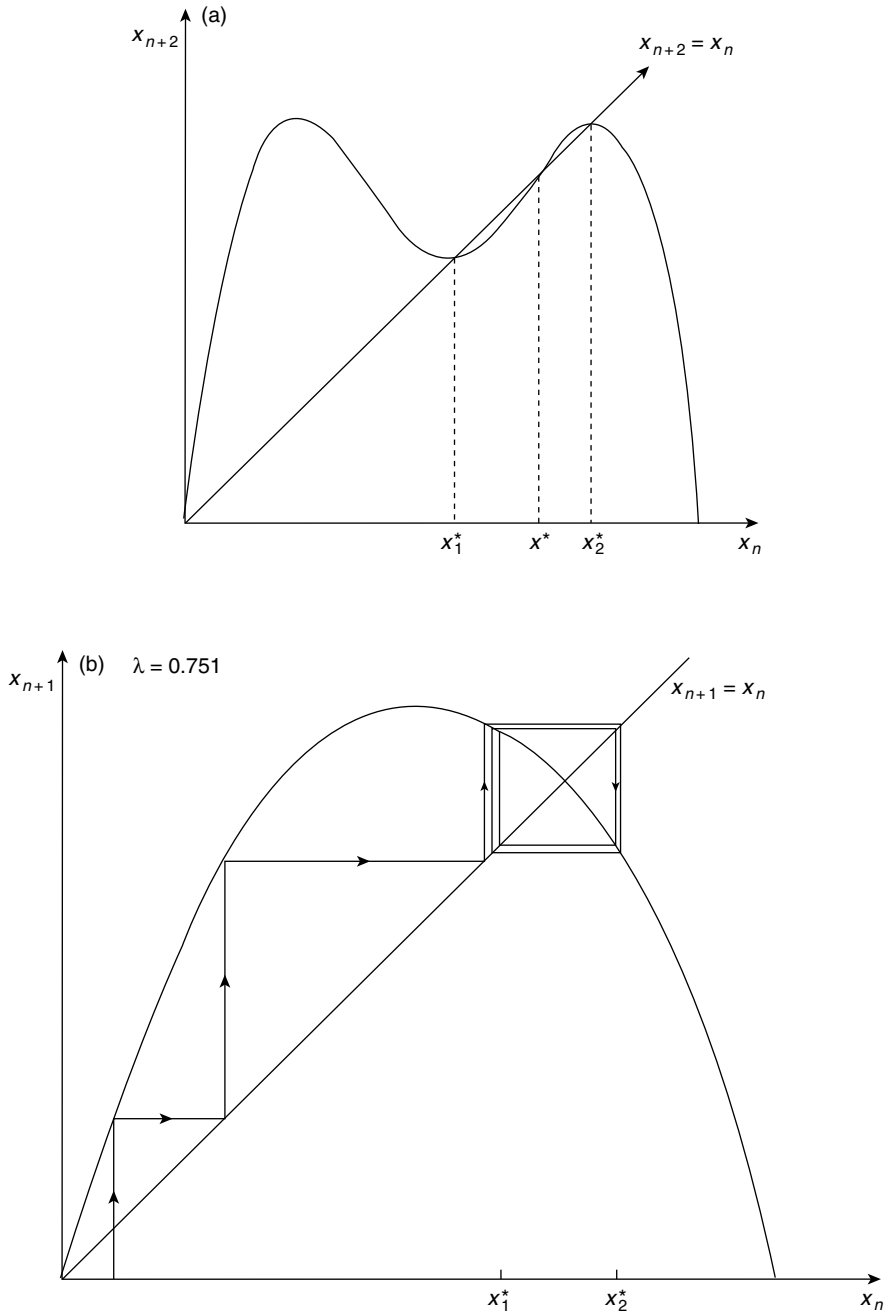


**Figure 14.11** (a)  $x_1^*$  and  $x_2^*$  are two of the three fixed points formed by the intersection of  $x_{n+2} = f^2(x_n)$  and its bisector  $x_{n+2} = x_n$ . The third fixed point is the original fixed point  $x^* = 1 - \frac{1}{4\lambda}$  of  $x_{n+1} = f(x_n)$ . (b) When the value of  $\lambda$  is just greater than  $\frac{3}{4}$  period doubling begins between two new fixed points  $x_1^*$  and  $x_2^*$

The stable fixed points  $x_1^*$  and  $x_2^*$  of  $f^2(x)$  for  $\lambda > \frac{3}{4}$  are not fixed points of  $f(x)$ . Clearly, since these points lie on the bisector  $x_{n+2} = x_n$ , each will return to itself every second iteration. This can occur only when the expressions

$$x_1^* = f(x_2^*) \quad \text{and} \quad x_2^* = f(x_1^*)$$

jointly hold so a trajectory ends in the cycle  $x_1^* \rightarrow x_2^* \rightarrow x_1^* \rightarrow x_2^*$ , Figure 14.11(b).

**(Problem 14.6)**

In the same way that  $x_1^*$  and  $x_2^*$  became the two stable points at  $\lambda_1 = \frac{3}{4}$  they will become simultaneously unstable for some larger value  $\lambda_2$  when  $f^{2'}(x^*) = -1$ . At  $\lambda_2$ ,  $x_1^*$  and  $x_2^*$  will each bifurcate to two stable points to give a stable 4-cycle period based on the stable fixed points of  $f^4(x)$ . As the period doubling sequence continues, via pitchfork bifurcations, the values  $\lambda_1, \lambda_2, \lambda_3, \lambda_4 \dots$  for the cycles  $2, 2^2, 2^3, 2^n \dots$  converge geometrically and Feigenbaum (1978) found that for this period doubling sequence the limit as  $n \rightarrow \infty$  is given by

$$\delta_{n \rightarrow \infty} = \frac{\lambda_{n+1} - \lambda_n}{\lambda_{n+2} - \lambda_{n+1}} = 4.6692016$$

This result appears to be verified not only for the logistic map but for other non-linear equations with a single maximum and many experiments, computer simulated and otherwise, support Feigenbaum's result.

The value of  $\lambda$  at which the cycle  $2^n (n \rightarrow \infty)$  is approached is given by  $\lambda_\infty = 0.8925$ . This is illustrated in Figure 14.12 where the successive bifurcations of  $2^n$  cycles become

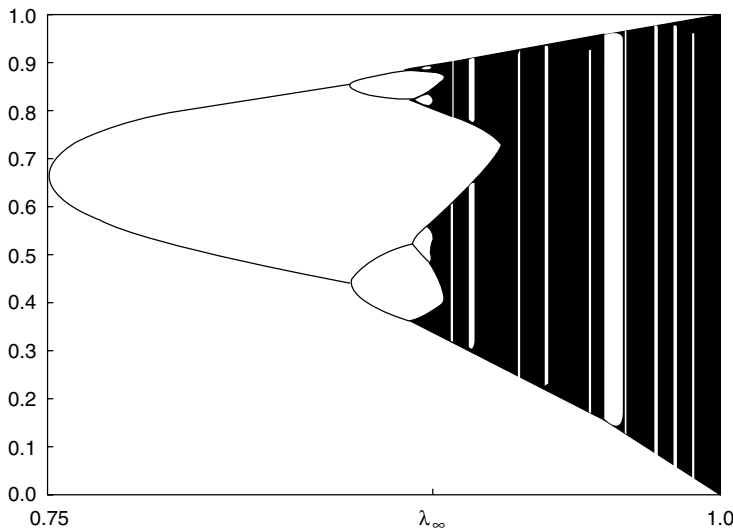


**Figure 14.12** Bifurcations at period doubling for the logistic map begin at  $\lambda = \frac{3}{4}$  and reach the limit  $2^\infty$  at  $\lambda_\infty$ . Between  $\lambda_\infty$  and  $\lambda = 1$  chaotic behaviour is interspersed with regions or windows at which odd numbered cycles of period  $k$  and their harmonics  $k2^n$  appear. Some cycles are aperiodic (Figure 14.13). (From Tabor, 1989)

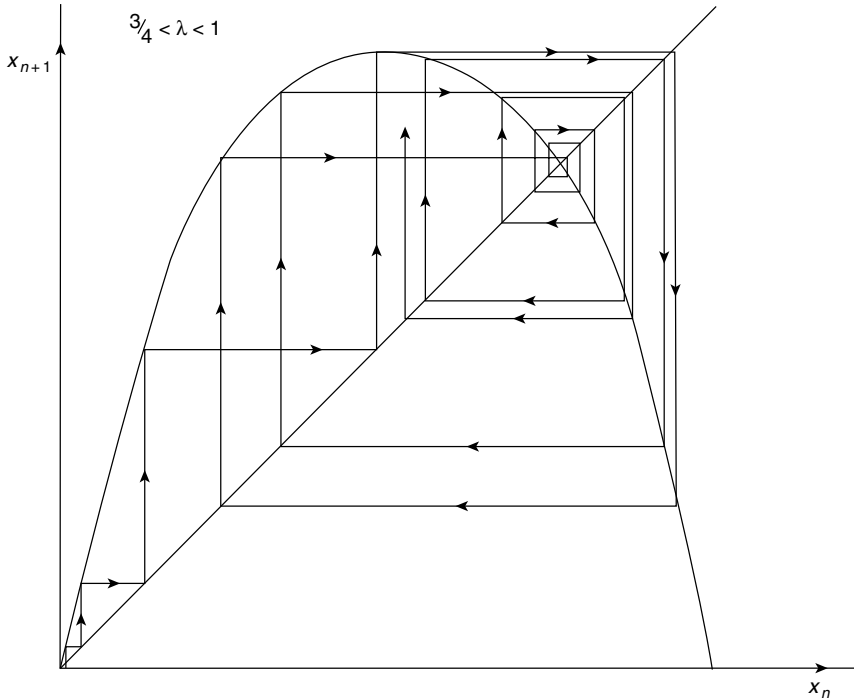


**Figure 14.13** An aperiodic cycle which remains bounded within the system for  $\frac{3}{4} < \lambda < 1$

increasingly compressed in the  $\lambda$  space. Between the values of  $\lambda_\infty$  and  $\lambda = 1$  a very rich behaviour is observed; there is an infinite number of different periodicities and an uncountable number of very long cycles of no measurable period but which remain bounded within the system (Figure 14.13).

The order in which these cycles appear has been successfully predicted by Metropolis *et al.* (1973). The first odd cycle appears at  $\lambda = 0.9196$  and the first period 3 cycle appears at  $\lambda = 0.9571$ . This is an important cycle because of the paper by Li and Yorke entitled ‘Period 3 implies Chaos’ (Li and Yorke, 1975).

We can examine the origin of the first period 3 cycle in Figure 14.14(a). At some value  $\lambda^*$  the bisector  $x_{n+3} = x_n$  is tangent to the curve  $x_{n+3} = f^3(x_n)$  at the three fixed points  $x_1^*$ ,  $x_2^*$ ,  $x_3^*$ . The slope of  $f^3(x_n)$  at these points must equal +1 and each of these three unstable fixed points bifurcates into a pair of which one is stable and the other is unstable. This is the tangent bifurcation. The period 3 cycle orbits between the three stable fixed points (one from each bifurcation) and we can follow the bifurcation process by increasing  $\lambda$  beyond  $\lambda^*$  by a small quantity. This heightens the maxima and deepens the minima so that the bisector now cuts  $f^3(x_n)$  in pairs of points one on each side of the tangent position. A typical pair is shown in Figure 14.14(b) on a magnified scale. The tangent point T splits into points A and B each of which moves along the curve from T as  $\lambda$  increases. Point A moves from a gradient position of +1 around the curve maximum to a gradient position of less than 1 and forms the stable fixed point of the bifurcated pair. Point

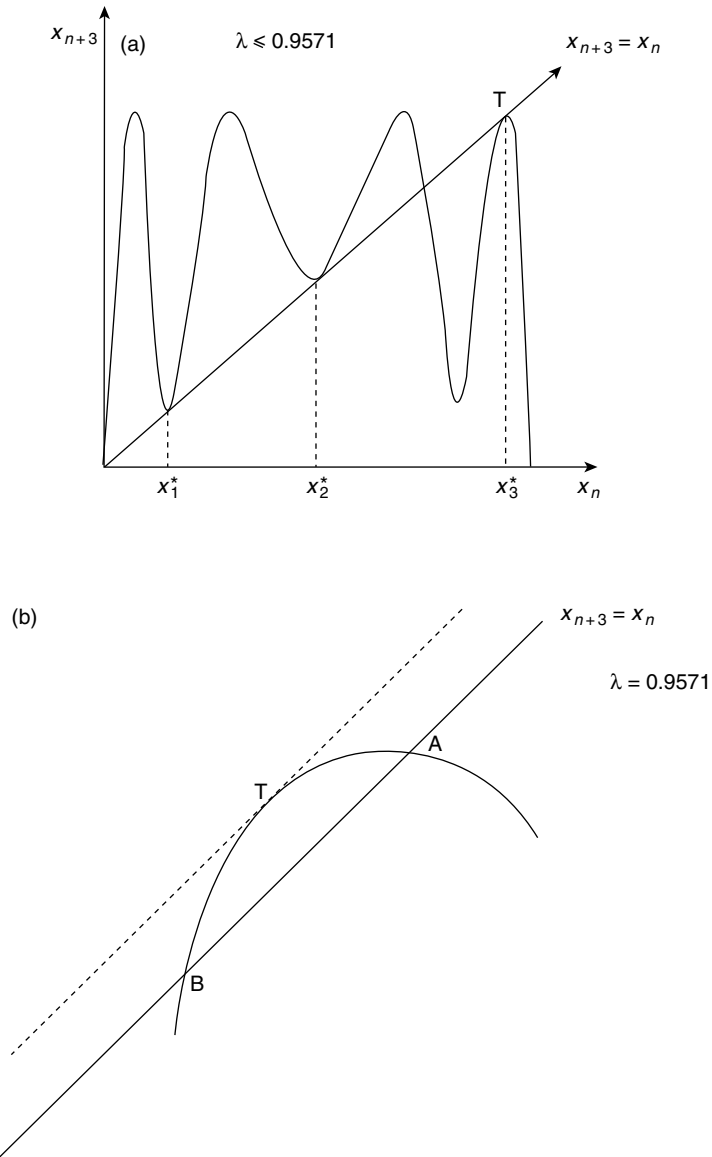


**Figure 14.14** (a) The first period 3 cycle appears at  $\lambda = 0.9571$ . Just below this value of  $\lambda$  the bisector  $x_{n+3} = x_n$  is tangent to  $x_{n+3} = f^3(x_n)$  at three unstable fixed points (gradient = +1). A small increase of  $\lambda$  splits these points into pairs, one point of each pair becoming stable. (b) Magnification at tangent point T which splits into a pair A and B with a small increase in  $\lambda$ . At T the gradient is +1 (unstable), A is stable at a reduced gradient and B is unstable at an increased gradient

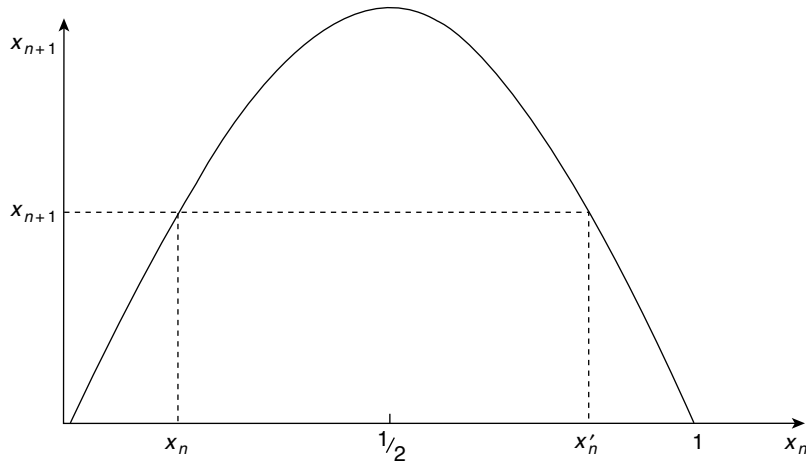


**Figure 14.15** The one-dimensional logistic equation  $x_{n+1} = 4\lambda x_n(1 - x_n)$  is non-invertible because trajectories cannot be traced uniquely backwards to their origins. Each  $x_{n+1}$  can arise from two different values of  $x_n$

B moves from T (gradient +1) along the curve to a steeper gradient position and remains unstable.

Thus, to quote May, ‘the fundamental stable dynamical units are of basic period  $k$  which arise by tangent bifurcation along with their associated cascade of harmonics of periods  $k2^n$  which arise by pitchfork bifurcation. The hierarchy of stable cycles of period  $2^n$  (namely,  $k = 1$ ) is merely a special case albeit a conspicuously important one’.

The one dimensional logistic map has one profound limitation. Figure 14.15 shows that it is symmetric about the point  $x = \frac{1}{2}$  so that any  $x_{n+1}$  can arise from one of two different values  $x_n$  and  $x'_n$ . This fails an essential requirement in chaos theory, namely that all trajectories may be traced uniquely backwards in time to their origins. This property is known as ‘invertibility’ and clearly the logistic map is non-invertible.

## Chaos in a Non-linear Electrical Oscillator

The development of the varactor has made it possible to display many features of the preceding section on a cathode ray oscilloscope in a first year university laboratory experiment. The varactor acts as a diode in the forward direction but behaves in the reverse direction as a variable non-linear capacitance in a series LCR circuit. Testa *et al.* (1982) confirmed not only many of the results above but, in addition, supported two predictions made by Feigenbaum (1979). These were

1. That bifurcation at period doubling follows a distinct procedure—as a  $2^n$  cycle loses stability after  $2^n$  iterations, a point of the attractor just misses duplicating itself with duplication occurring only after another  $2^n$  iterations. Thus each element of the cycle splits into closely spaced pairs with  $2^n$  iterations required to visit an element from its

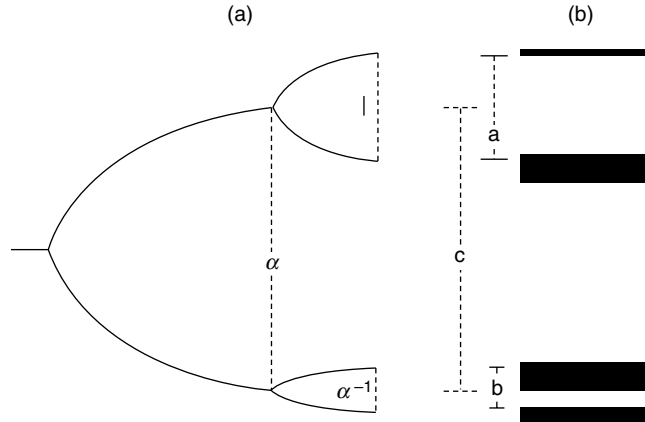


**Figure 14.16** In the period doubling process the separation of adjacent elements in a pair is reduced by a universal factor  $\alpha$  from one bifurcation to the next. For period doubling between 16 and 32  $\alpha = a/b = 2.35$  and  $\alpha = c/a = 2.61$ . Reproduced by permission of The American Physical Society from Testa *et al.* (1982)

adjacent neighbour. From one bifurcation to the next, separation of adjacent elements in a pair is reduced by a universal factor  $\alpha = 2.5029$  (Figure 14.16).

2. After a spectral component in the period doubling process has been generated, its amplitude remains approximately constant during further bifurcation and each new subharmonic of this frequency can be predicted as having its amplitude reduced by  $10 \log_{10} \mu$  where

$$\mu = \frac{4\alpha}{(2 + \frac{1}{\alpha^2})^{1/2}} = 6.57$$

A typical varactor LCR circuit is shown in Figure 14.17 with the non-linear capacitance given by

$$C(V) = C_0 / (1 + V_c / \beta)^\gamma$$

where  $V_c$  is the voltage across the varactor. In Testa's experiment  $C_0 = 300$  pF,  $\beta = 0.6$ ,  $\gamma = 0.5$ ,  $L = 10$  mH and  $R = 28 \Omega$ . For low values of  $V_0$  this gave a high  $Q$  resonance circuit at a frequency of 93 kHz. With  $f$  fixed near the resonance frequency in the driving voltage  $V_0 \sin 2\pi ft$ ,  $V_0$  was varied and the varactor voltage  $V_c(t)$  was measured. Testa *et al.* assumed that  $V_0$  played the role of  $\lambda$  in the logistic equation and that  $V_c$  corresponded to  $x$ . A real time display on a double beam CRO of  $V_c(t)$  and  $V_0(t)$  clearly revealed threshold values of  $V_{0n}$  for bifurcations into subharmonics  $f/n$  where  $n = 2, 4, 8, 16$ . At  $n = 4$  (not shown by Testa) this would appear as Figure 14.18.

Figure 14.19 was obtained on the oscilloscope screen by Testa with a slow horizontal scan of  $V_0$  versus the varactor voltage  $V_c$  which was magnified in selected steps of 10 mV. The numbers on the horizontal axis indicate the generation of particular periods and

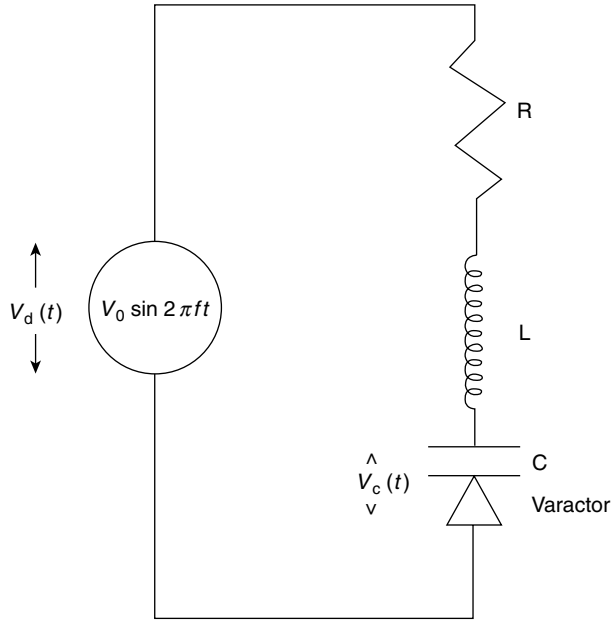


**Figure 14.17** Non-linear LCR series circuit where the non-linear element is the varactor C which acts as a diode in the forward direction but becomes a variable non-linear capacitance in the reverse direction

bifurcations are clearly visible. The threshold values of  $V_0$  for these periods are shown in Table 14.1. The first four threshold values  $V_{0n}$  gave

$$\delta_1 = \frac{V_{02} - V_{01}}{V_{03} - V_{02}} = 4.257 \pm 0.1$$

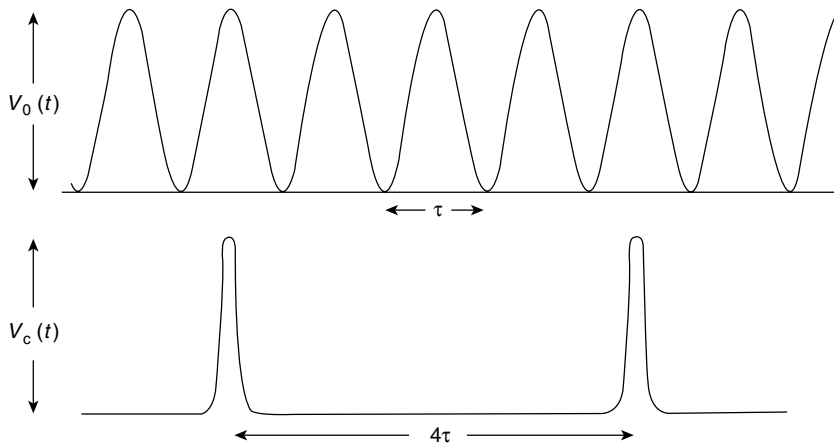


**Figure 14.18** Double beam oscilloscope showing driving voltage  $V_0(t)$  at frequency  $f$  and varactor voltage  $V_c(t)$  at frequency  $f/4$ . Values of  $V_{0n}$  for appearance of  $f/n$  are given in Table 14.1

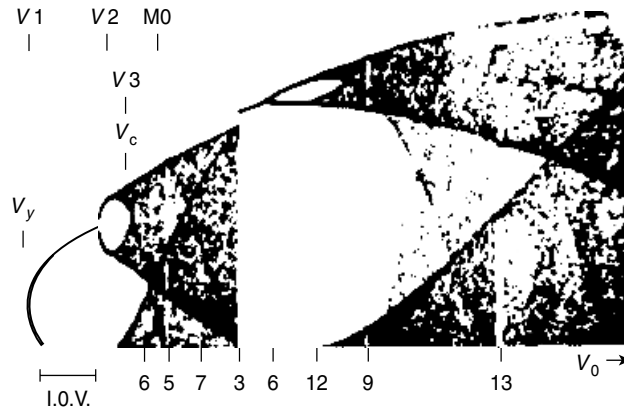


**Figure 14.19** Slow horizontal scan of  $V_0$  versus  $V_c$ . The numbers on the horizontal axis indicate the generation of particular periods. Bifurcations are clearly visible. Threshold values of  $V_0$  for various periods are shown in Table 14.1. Reproduced by permission of The American Physical Society from Testa *et al.* (1982)

**Table 14.1** Table of periods and the threshold values  $V_0$  at which they appear

Period	Threshold $V_0$ (rms volts)	comments
2	0.639	} Threshold for periodic bifurcation
4	1.567	
8	1.785	
16	1.836	
32	1.853	
Chaos	1.856	Onset of noise
12	1.901	} Window
24	1.902	
6	2.073	} Window
12	2.074	
5	2.353	} Window
10	2.363	
7	2.693	} Window
14	2.696	
3	3.081	} Wide Window
6	3.338	
12	3.711	
24	3.821	
9	4.145	
18	4.154	} Window

Reproduced by permission of the American Physical Society from Testa *et al.* (1982)

and

$$\delta_2 = \frac{V_{03} - V_{02}}{V_{04} - V_{03}} = 4.275 \pm 0.1$$

in the Feigenbaum convergence series.

To test the first of Eigenbaum's predictions the values of  $c$ ,  $a$  and  $b$  in Figure 14.16 were measured for the bifurcations between periods 16 and 32. These gave

$$\alpha = \frac{a}{b} = 2.35 \quad \text{and} \quad \alpha = \frac{c}{a} = 2.61$$

As periods doubled the power reduction in their frequency components was measured and the results were consistent with Feigenbaum's analysis.

## Phase Space

One of the most vital concepts in the description of chaos is that of phase space. In one dimension, e.g. the logistic equation, trajectories can be followed without introducing it. In higher dimensions it is essential.

The idea of phase space has many applications in physical sciences. Students meet it initially in the Maxwell–Boltzmann statistical distribution where the question is asked: 'Given  $N$  gas particles at a temperature  $T$  occupying a volume  $V$ , what fraction of  $N$  will be found in the velocity range  $v$  to  $v + dv$  in the small volume range  $dV$ ?' We shall discuss this application to statistical distributions in an appendix at the end of the book.

The number of dimensions of phase space is determined by the number of coordinates required to define the complete physical state of the system. For each gas particle above we need six dimensions, three for the  $v_x, v_y, v_z$  components in velocity space and three for the  $x, y, z$  components in the configuration space  $V$ .

Each point in phase space defines the complete physical state of the system (here a gas particle) and trajectories in phase space follow the physical development of the system.

When the energy of an ensemble of systems (particles) is conserved the phase space or volume associated with them remains constant, but if any energy is dissipated the phase volume contracts. This contraction generates a sub-space, there is a reduction in the number of coordinates required and their range is reduced.

Figures 14.20–14.23 show, in turn, the two dimensional phase space diagrams of different oscillators using the coordinates  $\dot{x}$  and  $x$ .

1. A linear simple harmonic oscillator (Figure 14.20).
2. a damped simple harmonic oscillator (Figure 14.21).
3. an undamped non-linear oscillator formed by a pendulum supported on a light rigid rod (Figure 14.22)
4. (a) an undamped oscillator with a potential energy

$$V = -\frac{1}{2}ax^2 + \frac{1}{4}bx^4$$

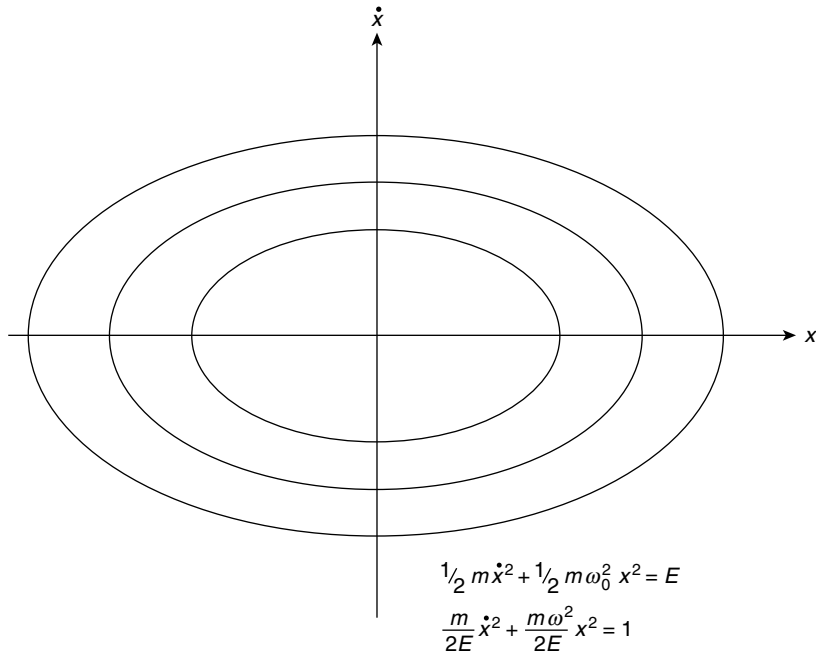


**Figure 14.20** Linear simple harmonic oscillator represented in the two dimensional phase space of  $\dot{x}$  and  $x$ . Each ellipse corresponds to a curve of constant energy and encloses a constant area of phase space

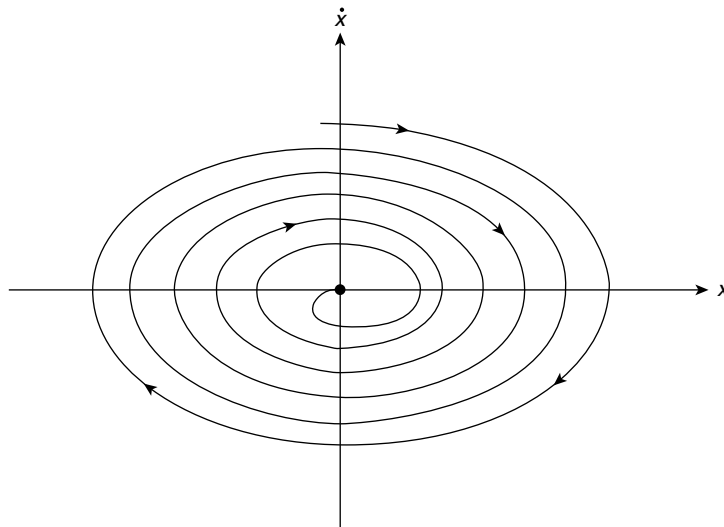


**Figure 14.21** The energy loss per cycle in a damped simple harmonic oscillator is shown in its phase space diagram as a reduction of area with each cycle as its trajectory spirals to a stable point attractor at the origin

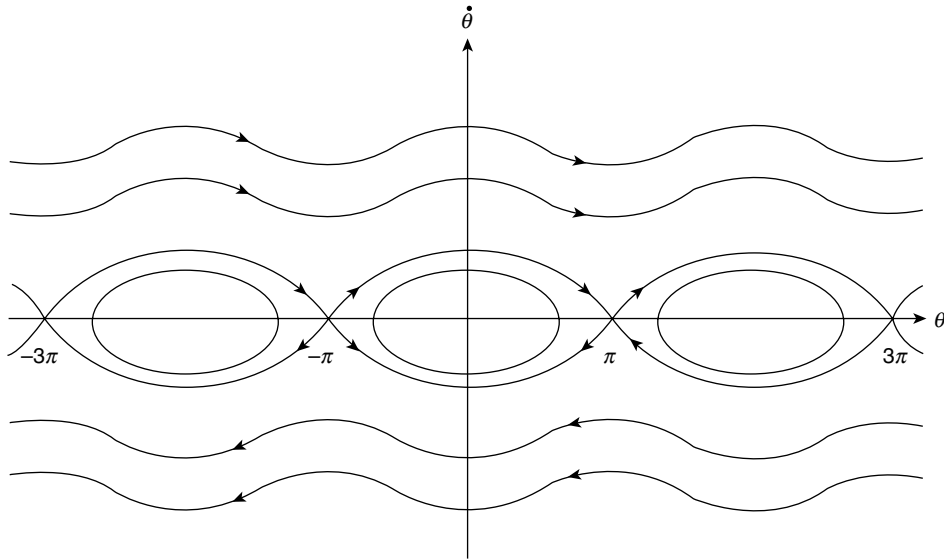


**Figure 14.22** Phase portraits for a non-linear pendulum on a light rod. The closed curves represent energy values up to the limit  $\dot{\theta} = 0$  at pendulum amplitude  $\theta = \pm\pi$  ( $\theta = 0$  is the hanging rest position). The open curves represent fast rotations with energy values large enough for  $\dot{\theta} > 0$  at  $\theta = (2n + 1)\pi$

(b) the oscillator of 4(a) now lightly damped (Figure 14.23).

The features of each will now be described, introducing ideas which are frequently met in chaotic systems.

1. The trajectory in  $\dot{x}$  phase space for a simple harmonic oscillator of constant energy is an ellipse of constant area. Its potential energy curve is the familiar parabola of p. 10.
2. For a lightly damped simple harmonic oscillator where energy is dissipated the phase space is an inward spiral on to the equilibrium zero position which is a stable point attractor. As energy is lost each orbit of the spiral encloses a smaller element of phase space than its predecessor, unlike (1).
3. Here we plot the phase portraits for a large range of pendulum energies  $E$ . The closed curves represent those energy values up to the limit where the pendulum (rigid rod) stands on its head with zero velocity and angular amplitude  $\theta = \pm\pi$  measured from the hanging rest position. Higher  $E$  values have open curves because their rotations are fast enough to pass through the values of  $\theta = (2n + 1)\pi$  with velocities  $\dot{\theta} > \dot{\theta}$ . The largest closed curve has pointed ends, at maximum amplitude  $\theta$ , because  $\dot{\theta}$  is small for changes of  $\theta$  in that range. Each interval of  $2\pi$  along the horizontal axis represents a complete rotation.

The curves passing through  $\theta = \pm\pi$  evidently separate those energies capable of allowing complete rotations from those which cannot. Such a curve is called a separatrix and the points  $\theta = \pm\pi$  are called saddle points.

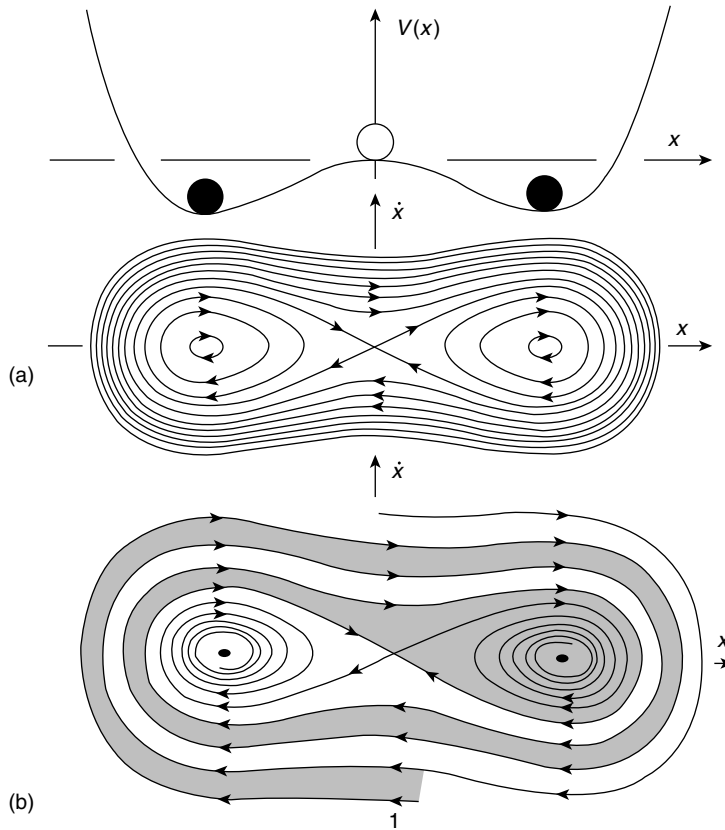


**Figure 14.23** Potential energy curve  $V = -\frac{1}{2}ax^2 + \frac{1}{4}bx^4$  with phase portraits for the damped and undamped oscillators. For the undamped oscillator energies  $V(x) < 0$  restrict the motion to that potential well containing the  $\dot{x}$  starting position. (a) When the starting position is on the curve  $V(x) > 0$  the trajectories cross the potential barrier repeatedly. (b) For the damped oscillator trajectories from a given range of  $\dot{x}$  starting positions will finish at the bottom of a particular potential well (indicated by the shaded region known as the basin of attraction). The other basin of attraction is unshaded. Reproduced by permission of John Wiley & Sons from Thompson and Stewart (1986)

4. The potential energy curve  $V = -\frac{1}{2}ax^2 + \frac{1}{4}bx^4$  is drawn together with the phase portraits for the undamped and damped oscillators. For the undamped oscillator any starting position with total energy less than  $V(x) = 0$  restricts the motion to one or other of the potential wells. For any starting position greater than  $V(x) = 0$  the motion may cross the potential barrier repeatedly. The trajectory associated with motion starting from rest at any of the three  $V(x) = 0$  positions is the separatrix through the saddle point.

If the oscillator now has a small damping term  $r\dot{x}$  the final rest position is determined exclusively by its starting values  $\dot{x}$  and  $x$ . The saddle connection is broken and the two equilibrium states are now competing point attractors. Starting positions of  $(\dot{x}, x)$  which lie in the dotted regions of the phase space generate trajectories which will come to

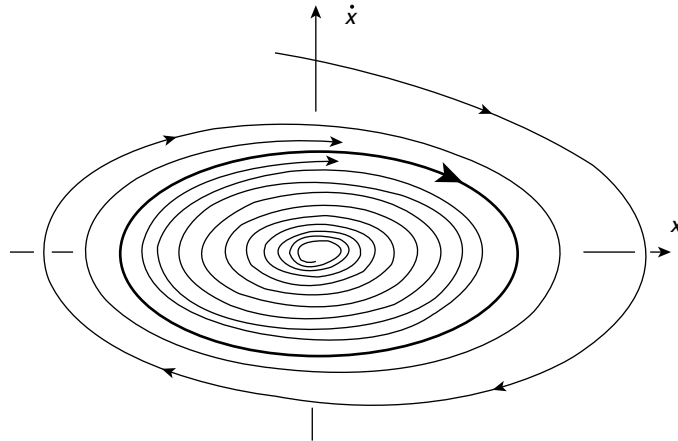


**Figure 14.24** Repellor and limit cycle. Phase trajectories of an oscillator governed by the equation  $m\ddot{x} - r\dot{x} + d\dot{x}^3 + sx = 0$ . For  $x$  small and  $r$  positive, trajectories spiral outwards from the repellor at the origin. For large  $\dot{x}$ , the  $d\dot{x}^3$  term dominates and trajectories spiral inwards. These effects balance at some boundary to form a stable limit cycle. Reproduced by permission of John Wiley & Sons from Thompson and Stewart (1986)

equilibrium in the dotted attractor spiralling to rest at the minimum of the right hand potential well. Similarly the clear region of phase space defines the starting positions and trajectories which will finish at the minimum of the left hand potential well. Each of these two phase space regions is called a *basin of attraction*.

## Repellor and Limit Cycle

To illustrate the concepts of repellor and limit cycle in two dimensional phase space we consider the damped non-linear oscillator governed by the equation

$$m\ddot{x} - r\dot{x} + d\dot{x}^3 + sx = 0$$

When  $x$  is very small we can neglect the  $d\dot{x}^3$  term and if  $r$  is positive we have negative damping giving outwardly spiralling trajectories from the central point which is therefore a repellor. For large values of  $\dot{x}$ ,  $d\dot{x}^3$  is the dominant term and the trajectories spiral inwards. These competing effects are balanced at some boundary to form a steady state oscillation in a stable limit cycle of fixed period, Figure 14.24.

## The Torus in Three-dimensional $(\dot{x}, x, t)$ Phase Space

Extending the ideas about phase space let us consider the generation of a torus by following the trajectory of a particle (or system) subject to the influence of two perpendicular circular simple harmonic motions of angular frequencies  $\omega_0$  and  $\omega_1$ , where  $\omega_0$  traces a circle in the azimuthal plane with a radius  $r_0$  while  $\omega_1$  causes the particle to spiral on the surface of a torus of radius  $r_1$  (Figure 14.25). A cross section of the torus will be a circle of radius  $r_1$ ,

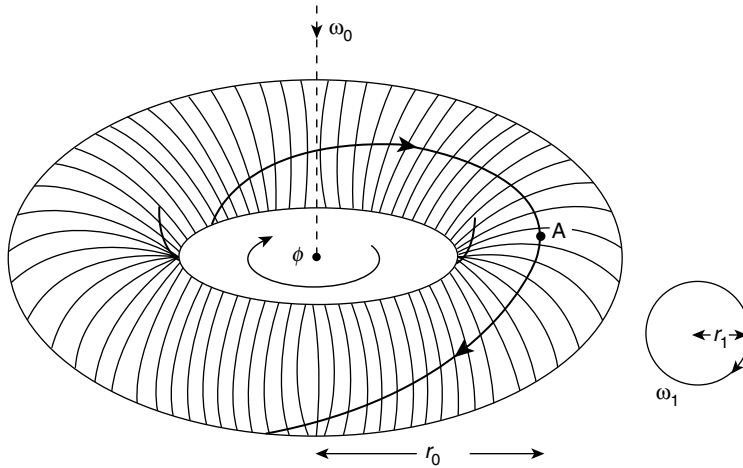


**Figure 14.25** Torus in  $(\dot{x}xt)$  phase space generated by a system subject to the influence of two perpendicular circular simple harmonic motions. The trajectory of the system spirals on the torus surface

and the particle will register some point on the circumference of the circle each time it passes the cross section. If  $\omega_1 = \omega_0$  this point will be identical for each period  $\tau_0 = 2\pi/\omega_0$ . However, if  $\omega_1 \neq \omega_0$  the particle will arrive at different points on the circle circumference after each interval  $\tau_0$ ; for example, if  $\omega_1 = 3\omega_0/4$ , the particle will travel only  $\frac{3}{4}$  of the circumference for each  $\tau_0$  and will register the points A B C D of Figure 14.26 in that order.

Such a cross section is called a Poincaré section in phase space and is a vital tool in describing the multiple excursions of trajectories in phase space associated with chaos. It is always taken at some fixed interval of the system such as  $\tau_0$ , a typical example, as we shall see, is the period of the force driving an oscillator displaying chaotic motion.

The Poincaré section for a simple harmonic oscillator taken in the upper half plane containing the  $\dot{x}$  axis but normal to the  $x$  axis consists of only one spot at the maximum value of  $\dot{x}$  as the system passes through this position at intervals of  $\tau_0$ . A similar section for the damped oscillator will register a series of points between  $\dot{x}$  maximum and the origin as the trajectory spirals inwards.

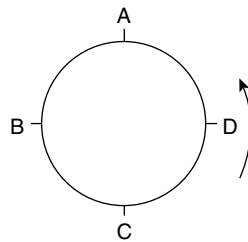


**Figure 14.26** When  $\omega_1 = 3\omega_0/4$  in Figure 14.25, the system will register the points ABCD in that order at a given cross section. This is an example of a Poincaré section in phase space

If the motion associated with  $\omega_1$  is not circular the surface of the torus will be distorted. We shall see that it can be pulled out, crinkled and folded back on itself so that its Poincaré section will assume remarkable shapes. When the repeated excursions of trajectories are located on such a surface it is called a manifold. The final state of such a distorted surface represents the reduced phase space which follows the dissipation of energy. Within this space is located the attractor to which the orbiting trajectories are bound.

## Chaotic Response of a Forced Non-linear Mechanical Oscillator

Fifty years ago no engineer calculating the forced vibrations of a beam via the equation

$$\ddot{x} + k\dot{x} + x^3 = B \cos t$$

could have foreseen the complexity of response which computer simulated solutions have uncovered. Ueda (1980) has found no fewer than 21 distinct regions of behaviour using a range of  $B$  values (0–25) and  $k$  values (0–0.8) where the units are unspecified. Five of these 21 regions display chaos, the others contain a variety of different attractors. Thompson and Stewart (1986) have chosen particular  $B$  and  $k$  values from Ueda to illustrate many basic features of chaotic oscillators and the use of Poincaré sections to identify them. Even with the same  $B$  and  $k$  values the long term behaviour of the oscillator is found to depend critically upon the starting values of  $\dot{x}$  and  $x$  and Figure 14.27 shows the phase trajectories and wave forms of five stable periodic motions around attractors for  $B = 0.2$  and  $k = 0.08$  where the letter A denotes the starting point in each case.

We have already noted that one sign of impending chaos in a system is the divergence with time of phase trajectories from almost identical starting positions even though their behaviour is determined by the same equation. For a forced damped oscillator we saw on p. 58 that this behaviour consists of two terms, a transient which decays with time leaving the steady state component.

One of Ueda's chaotic regimens lies in the  $B$  range (6–8) and the  $k$  range (0.03–0.1) and Thompson and Stewart chose  $B = 7.5$  and  $k = 0.05$  for their illustration. Figure 14.28 shows phase trajectories of the oscillator for two almost identical starting positions labelled A and a of  $(\dot{x}, x)$ . Because the vibration waveform of the oscillator is so irregular there is only one way of registering the passage of time on this two-dimensional phase diagram and that is by marking off the constant period  $\tau_0$  associated with  $\cos t$  of the driving force. This gives points B and b and the trajectory divergence is already evident. This divergence may be traced over many periods of  $\tau_0$  and is found to be exponential with time. We can associate the points B and b and their successors after each interval of  $\tau_0$  with the formation of our Poincaré section of the torus on p. 489. Figure 14.29 shows the history of the single phase trajectory which started at A marked off in alphabetical order over the first nine periods of  $\tau_0$ . Note that each letter represents a maximum of the driving force  $B \cos t$  and that all letters fall on the right hand side of the  $\dot{x}$  axis, that is  $x$  positive.

Tracing this complicated trajectory on the three-dimensional  $(\dot{x}, x, t)$  phase surface of the torus would separate that is time resolve, the apparent trajectory crossing points in the two-dimensional picture. If now only the Poincaré section points A, B, C, D, etc. are plotted

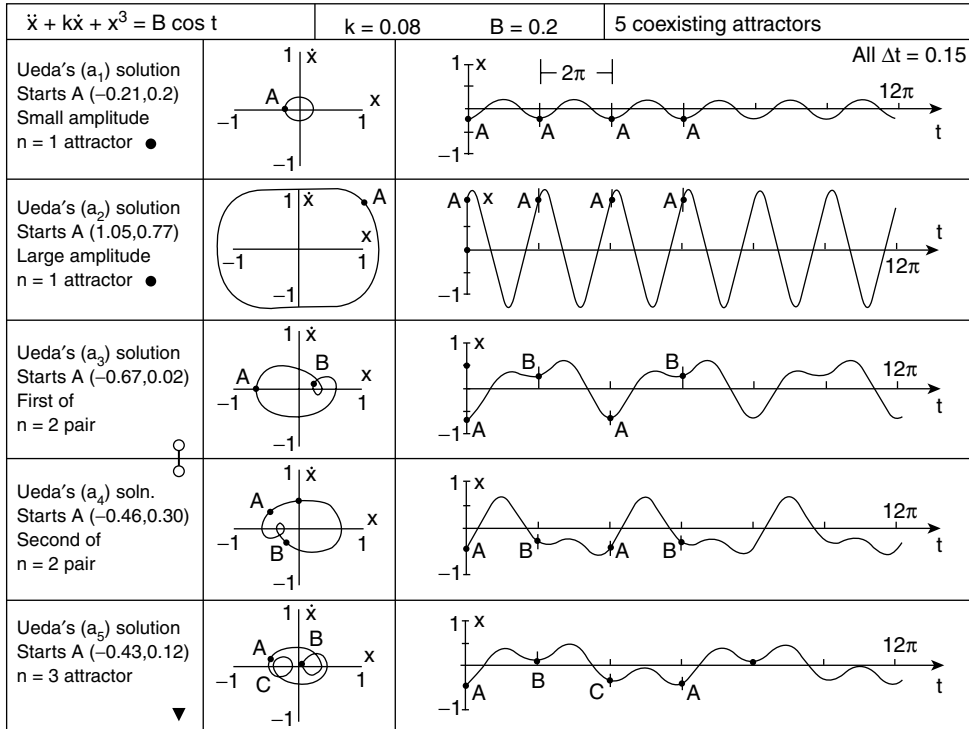


**Figure 14.27** Phase trajectories for the oscillator  $\ddot{x} + 0.08\dot{x} + x^3 = 0.2 \cos t$  are seen to depend critically upon the starting values of  $\dot{x}$  and  $x$ . The letter A denotes each starting position. Reproduced by permission of John Wiley & Sons from Thompson and Stewart (1986)

over a very large number of intervals of  $\tau_0$  they build up a shape of which that shown in Figure 14.30 is typical.

Irrespective of any starting position or of the size and duration of any transients all long term, steady state, Poincaré section points eventually settle to contribute to this pattern. It bears the signature of a chaotic attractor for high resolution displays a fine structure known as fractal. It is an example of the stretching and folding of an ensemble of steady state trajectories in phase space during which the trajectories become thoroughly mixed; that is, change from one set of close neighbours to another. The important point is that despite mixing, the trajectories retain their distinct identities and never merge; their time histories are invertible.

### A Brief Review

We now review briefly the discussion so far in order to present a clearer picture of what we shall expect to identify in following sections.

We saw on p. 474 how chaos could be approached via period doubling but that the symmetry of the population biology equation created an ambiguity on the route to chaos, so

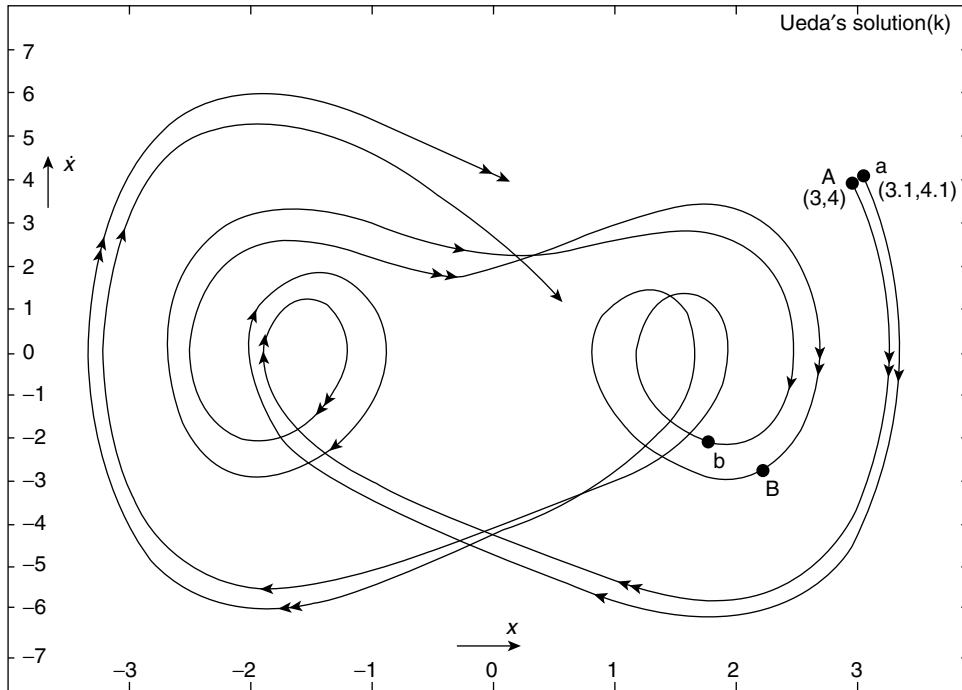


**Figure 14.28** Two phase trajectories from almost identical starting positions A and a for the oscillator  $\ddot{x} + 0.05\dot{x} + x^3 = 7.5 \cos t$ . After one period of the driving force the trajectories have diverged respectively to B and b. Reproduced by permission of John Wiley & Sons from Thompson and Stewart (1986)

that no final point on a trajectory could be uniquely time reversed back to its origin. This essential time reversal arises from the continuity of unique solutions to the non-linear equations governing the system. The solution at a given time defines the complete state of the system and occupies a point in phase space so that, with time, the trajectory traces a line in phase space. However, trajectories with close origins in a chaotic attractor system diverge exponentially with time while the energy dissipation always associated with chaotic attractors requires the phase space volume to contract. To reconcile these contradictory features, phase space of at least three dimensions is required and the problem is resolved essentially through stretching and folding this phase space. The distortion of phase space on a torus surface is an example of this.

To illustrate this process of stretching and folding, which we shall discuss later in more detail, we may consider two trajectories, originally close neighbours, which diverge as they spiral outwards on a plane (Figure 14.31) leaving the plane only to fold over by attraction and return back to the centre of the spiral. The divergence; that is, the sensitivity to initial conditions results from the stretching process and the folding comes from the attraction. The uniqueness of the trajectories in phase space ensures that they remain distinct, that they never merge, no matter how complex the phase space structure becomes. This complexity

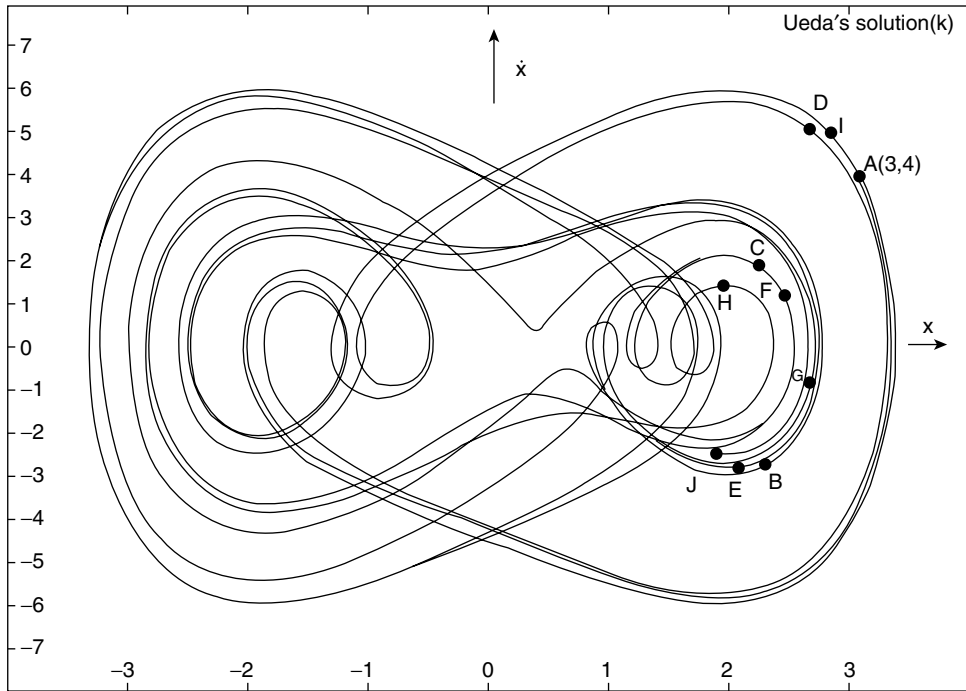


**Figure 14.29** A single phase trajectory traced over the first nine periods of the driving force in Figure 14.28. In three dimensional phase space the apparent crossing points would be separated by time resolution. Reproduced by permission of John Wiley & Sons from Thompson and Stewart (1986)

is revealed by the fractal nature of the highly resolved Poincaré section of the chaotic attractor in Figure 14.30.

We now explain what is meant by fractal structure and discuss how theories of phase space distortion or mapping produce it.

### Fractals

In topology a curve has a dimension of one and a surface a dimension of two. There are higher integral dimensions. The word 'fractal' was coined by Mandelbrot in 1975 to express the idea of a 'shape' with a non-integral dimension. He has since published books on the subject containing many beautiful computer generated patterns. The essential feature of all these fractal patterns is that they are self similar which means that, irrespective of scale, they retain the same geometric appearance. A well known example is the Koch snowflake.

### Koch Snowflake

Figure 14.32 shows an equilateral triangle of side length  $3l$ . On the central section of each side is placed a similar triangle of side  $l$  and the process is repeated indefinitely to produce

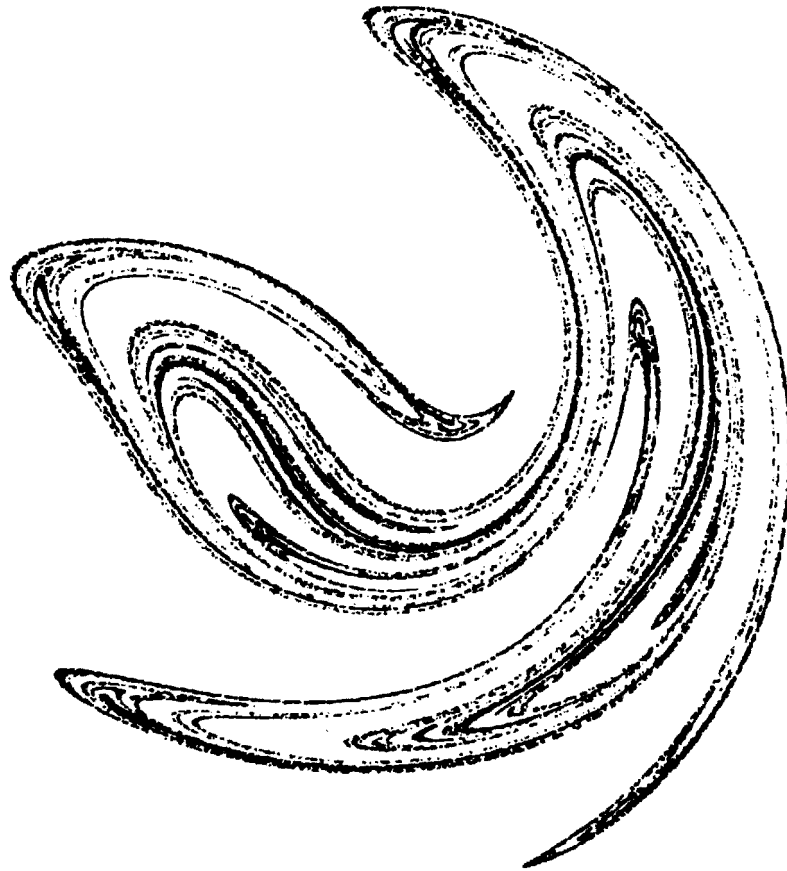


**Figure 14.30** Poincaré section for an oscillator similar to that of Figures 14.28 and 14.29. High resolution displays a fractal fine structure. Reprinted with permission from 'Steady motions exhibited by Duffing's equation: A picture book of regular and chaotic motions', by Yoshisuke Ueda, published in *New Approaches to Nonlinear Problems in Dynamics*, pp. 311--322. Copyright 1980 by the Society for Industrial and Applied Mathematics, Philadelphia, Pennsylvania. All rights reserved

a curve of infinite length ( $3l \times \frac{4}{3} \times \frac{4}{3} \dots$ ) but which encloses a finite area less than that of the circle surrounding the original triangle.

Mandelbrot was first led to the idea of fractals by studying noise on a transmission line. He found that the pattern or the distribution of the noise remained the same whether taken over a period of an hour, a minute or a second; that is, self similarity prevailed. He identified the pattern as belonging to a Cantor set which dates from the nineteenth century and which G. D. Birkhoff had suggested in the 1920s might be significant in dynamical systems.

#### *Cantor Set*

The Cantor set (Figure 14.33) is constructed by removing the centre part  $l$  of a line of length  $3l$  and repeating the process indefinitely. We define the total set of points lying on

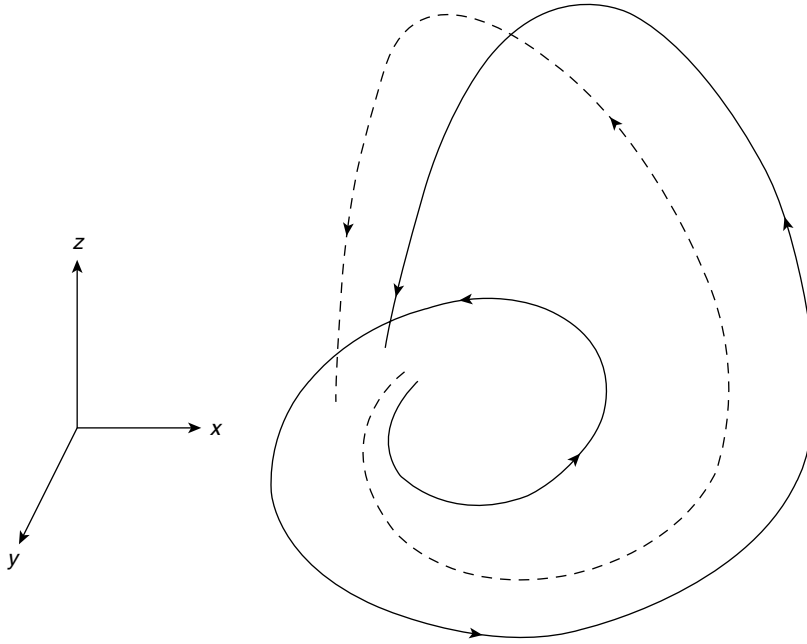


**Figure 14.31** Trajectories around a chaotic attractor diverge yet remain within a bounded region. This is achieved by the stretching and folding of phase space

the line segment  $l$  to be some function  $f(l)$  and assume this total set to be preserved so that

$$f(3l) = 2f(l)$$

If then  $f(l)$  is considered to vary as some power  $\delta$  of  $l$  so that  $f(l) \sim l^\delta$  we have  $f(3l) = 2f(l)$  giving  $(3l)^\delta = 2l^\delta$  so that  $3^\delta = 2$  and  $\delta = \log 2 / \log 3 = 0.6309$ . This is the non-integral fractal dimension of the Cantor set.

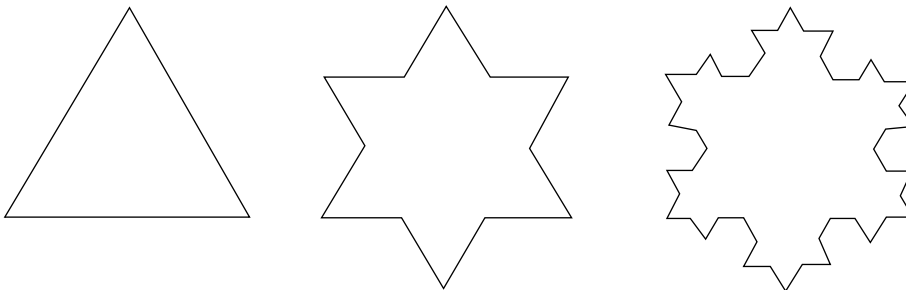


**Figure 14.32** The Koch snowflake has a fractal non-integral dimension. The final pattern has infinite length but encloses a finite area less than that of the circle surrounding the original triangle

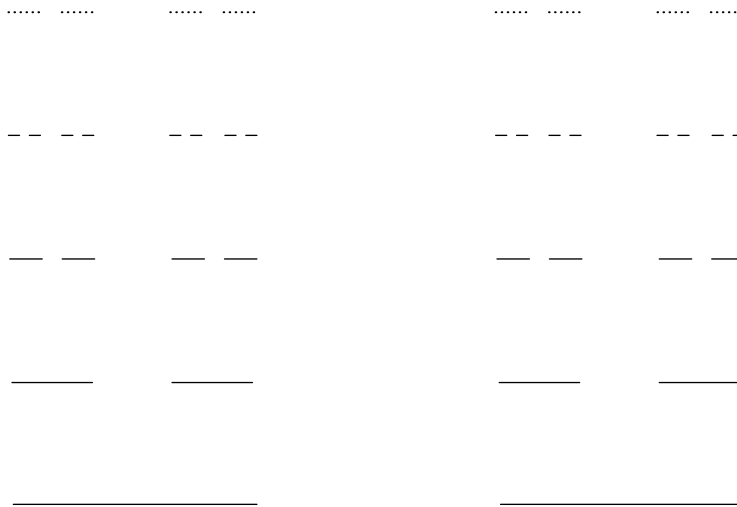


**Figure 14.33** A Cantor set has a fractal non-integral dimension and is produced by removing the central third of a line and repeating the process indefinitely with the remaining segments. Poincaré sections of chaotic attractors have a Cantor set-like structure

**(Problem 14.7)**

The importance of the Cantor set is that the highly resolved Poincaré section of a chaotic attractor such as that on p. 493 reveals a Cantor set-like structure. It results from stretching the phase space and folding it closely into layers. It is the signature of a chaotic attractor and we now look at how this may be achieved.

*Smale Horseshoe*

The mathematical process which describes the stretching and folding of phase space is called mapping and a number of such maps have now been devised to produce this effect, e.g. the Smale horseshoe (Smale, 1963).

In this example (Figure 14.34) a square is taken, stretched to double its length while its width is reduced to form a rectangle of area less than the square. The square may be taken as a cross section of a particular volume of phase space containing an ensemble or collection of trajectories the ends of which are shown as dots within the square. The reduction of area in the stretching process is equivalent to reducing the phase space by energy dissipation; at the same time it separates trajectories from their neighbours. The rectangle is then folded over into a horseshoe, the stretching and folding process is now repeated with the horseshoe again and again, so that successive cross sections reveal a Cantor set-like structure. The relative positions of the original trajectories are completely changed in this process.

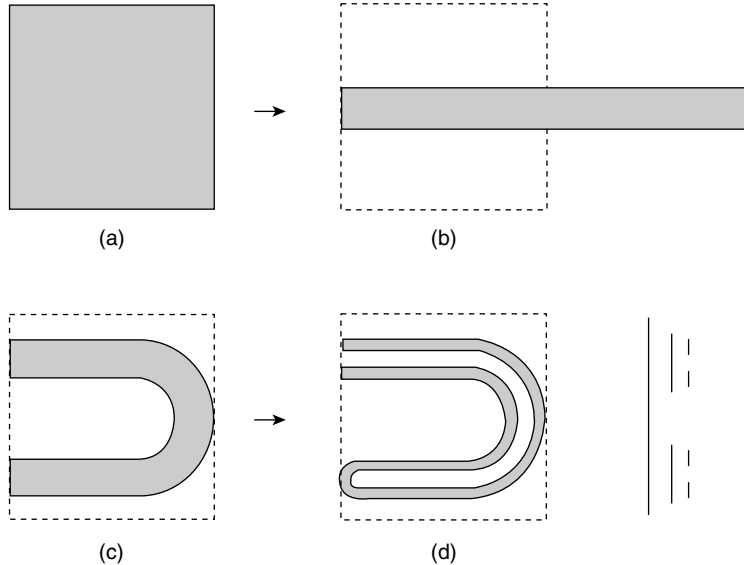


**Figure 14.34** The Smale horseshoe takes a square cross section of phase space containing an ensemble of trajectories (dotted ends), stretches the square to a rectangle of reduced area and folds the rectangle into a horseshoe. The process is repeated continuously with successive cross sections revealing a Cantor-set-like structure. The relative positions of the trajectories are changed in the process as the trajectories are mixed

## Chaos in Fluids

Turbulence in fluids is the most widely observed of all chaotic motions. Fast flowing water from a tap or around a blunt obstacle loses its low speed coherence and flow symmetry. A satisfactory description of the behaviour is made more difficult because:

- The theory of the liquid state is less well developed than that of gases and liquids.
- Experimental methods have until recently used probes which disturb the state of the system being measured.

The second of these difficulties has now been overcome by the development of laser-Doppler techniques combining the holographic system (p. 404) with the Doppler effect (p. 141).

Typically, a laser beam of frequency  $\nu_0$  and wavelength  $\lambda_0$  is split so that one half acts as a reference beam while the other is focused on a small fluid element ( $\sim 0.1$  mm diameter) moving with a velocity  $u$ . This beam is scattered through an angle  $\theta$  with a frequency  $\nu_s$ . The relationship between  $\nu_0$  and  $\nu_s$  is shown in Figure 14.35b. In Figure 14.35a the scattered beam joins the reference beam which is now modulated to give a component at the detector of the Doppler shift frequency  $\nu_D = \nu_s - \nu_0$ . If  $\mathbf{k}_0$  and  $\mathbf{k}_s$  are the wave number vectors associated respectively with  $\nu_0$  and  $\nu_s$  then the component of the velocity  $u$  parallel

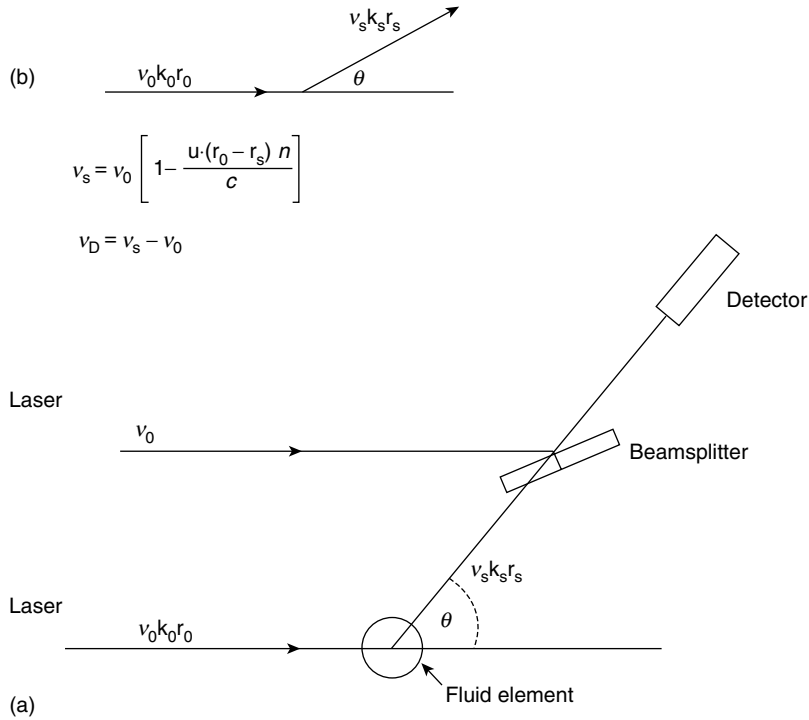


**Figure 14.35** (a) Scheme of the laser-Doppler technique for velocity measurements in a fluid. (b) The vector relationship between the scattered frequency  $\nu_s$ , the incident laser frequency  $\nu_0$  and the fluid velocity  $u$ ;  $r$  is a unit vector,  $n$  the refractive index of the fluid and  $c$  the velocity of light. The Doppler shift frequency is  $\nu_D = \nu_s - \nu_0$

to the vector  $\mathbf{k} = \mathbf{k}_0 - \mathbf{k}_s$  depends only upon  $\lambda_0$ ,  $\sin \theta/2$  and  $\nu_D$ . Velocities in the range of  $10^{-6}$  to  $10^3 \text{ ms}^{-1}$  are capable of being measured by this system.

The frequency  $\nu_D$  is so much greater than the frequencies associated with the fluid motion that the measured  $u(t)$  gives an instantaneous velocity value. Continuous records of  $u(t)$  over long periods may be Fourier analysed to show sharply defined frequency components when the flow is periodic with the appearance of broad band noise when the flow becomes chaotic.

Chaos in fluids has been studied chiefly in two systems:

1. Couette flow where the appropriate parameter is the dimensionless Reynolds number.
2. Rayleigh–Bénard convection where the parameter is the dimensionless Rayleigh number. This system is the model used by Lorenz in finding the original strange attractor.

### Couette Flow

This flow was completely defined in the classic paper of G. I. Taylor (1923). In its simplest form it is produced in a fluid contained in the gap between two concentric cylinders with

radii differing by about a centimetre. One of the cylinders is fixed while the others rotates with an angular velocity  $\omega$  although sometimes both cylinders may rotate with different angular velocities. The outer cylinder is usually glass, allowing observation of the flow. At low speeds of angular rotation the flow is symmetric in the azimuthal direction (Figure 14.36a).

For flow in one dimension the relevant equation would read

$$\rho u_x \frac{\partial u_x}{\partial x} = \frac{-\partial p}{\partial x} + \frac{\mu \partial^2 u_x}{\partial x^2}$$

where  $\rho$  is the fluid density,  $u_x$  is the velocity in the  $x$  direction,  $p$  is the pressure and  $\mu$  is the fluid viscosity. Each term in the equation has the dimensions of force per unit volume; the left hand side term may be considered as an inertial force and the last term may be seen as the viscous force. Flow symmetry depends on the relative strengths of these forces and the Reynolds number is written dimensionally as

$$Re = \frac{\text{inertial force}}{\text{viscous force}} = \frac{\rho u^2 L^2}{L \mu u} = \frac{uL}{\eta}$$

where  $\eta = \mu/\rho$  is the kinematic viscosity and  $u$  and  $L$  are a characteristic velocity and length of the system.

For Couette flow

$$Re = \frac{r_1 \omega d}{\eta}$$

where  $r_1$  is the radius of the inner cylinder and  $d$  is the width of the cylindrical gap.

For slow speeds, that is low  $Re$ , any departure from symmetry is overcome by the viscous force restoring the system to equilibrium but as  $Re$  increases with increasing  $\omega$ , the inertial effects of any departure from symmetric flow may be too great for the restoring viscous force and purely azimuthal Couette flow is lost.

This loss of symmetry for high  $Re$  first shows itself as a series of vortices around each azimuthal flow line, so that fluid elements follow a spiral path in the azimuthal direction (Figure 14.36b). These vortices, called Taylor cells, are seen to arise as follows.

An elemental toroid of the fluid initially at radius  $r_1$ , circulating at angular velocity  $\omega_{r_1}$  is displaced to radius  $r_2$ . If its angular momentum is conserved we have

$$\omega_{r_1} r_1^2 = \omega'_{r_1} r_2^2$$

where  $\omega'_{r_1}$  is its new angular velocity. Its centrifugal force will exceed that of the fluid originally at  $r_2$  circulating with angular velocity  $\omega_{r_2}$  if

$$|\omega'_{r_1}| > |\omega_{r_2}|$$

Hence an instability develops if  $|\omega_{r_1} r_1|^2 > |\omega_{r_2} r_2|^2$  for  $r_2 > r_1$ ; that is, if

$$\frac{d}{dr} |\omega r^2| < 0$$

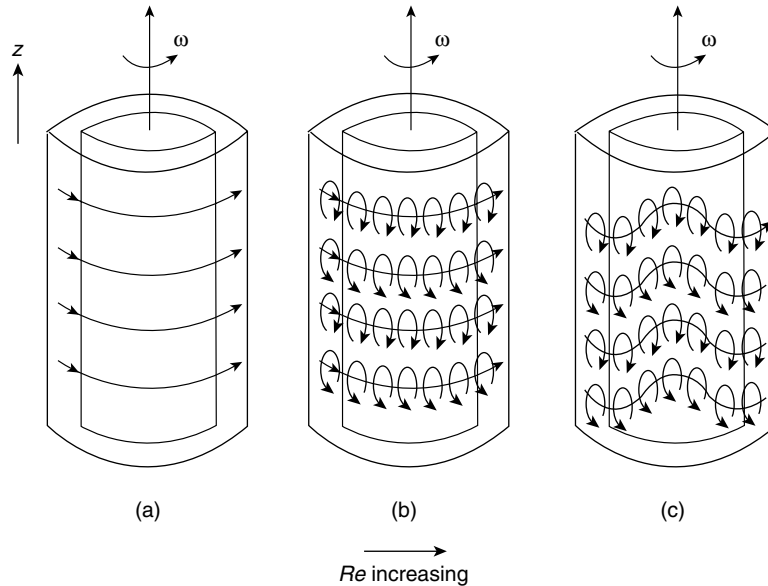


**Figure 14.36** In Couette flow a liquid is contained in the gap between two concentric cylinders one of which has an angular velocity  $\omega$  with respect to the other. At low Reynolds number  $Re$  the flow is azimuthal as in (a). As  $Re$  increases flow symmetry is lost and vortices develop (b). A further increase of  $Re$  develops transverse waves along the lines of vortices (c)

This is known as the Rayleigh criterion for the instability of Couette flow.

When the inner layers of the fluid are moving more rapidly than the outer layers they tend to move outwards because the centrifugal force is greater than the pressure holding them in place. A whole layer cannot move out uniformly because the outer layers are in the way so it breaks into cells which circulate.

The rotational motion of a fluid element in a Taylor cell appears as a periodic velocity variation in the  $z$  direction of Figure 14.36. Increasing  $Re$  that is the angular velocity of the cylinder, now causes harmonic oscillations of the vortices in the  $z$  direction as transverse waves travel around the azimuthal torus (Figure 14.36c). The frequency of these waves will be registered via the velocity measurements and as  $Re$  increases still more, other frequencies are generated and broad band noise begins to dominate with the appearance of chaos (Figure 14.37).

### Rayleigh–Bénard Convection

In this process heat provides the energy driving asymmetries in the flow. The incompressible fluid is contained between two horizontal plates about a centimetre apart, the lower of which is heated. For a small constant temperature difference between the plates the thermal conductivity and viscosity of the fluid ensure that the heat is conducted upwards in an orderly fashion (Figure 14.38a). When the temperature gradient is too steep the effect of these forces in maintaining equilibrium is overcome, flow symmetry is

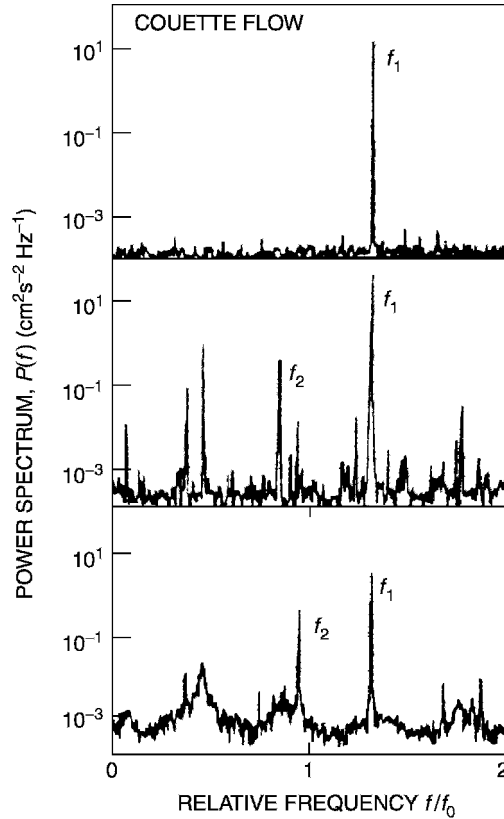


**Figure 14.37** The number of frequencies of the waves in Figure 14.36c increases with  $Re$  but broad band noise begins to dominate with the appearance of chaos in the bottom figure. Reproduced by permission of the American Institute of Physics from Swinney and Gollub (1978)

lost and convective rolls in both clockwise and anti-clockwise directions can develop (Figure 14.38b).

This occurs at some critical value of the Rayleigh parameter which we derive from the relevant equations. These are, in the positive  $z$  direction

$$\rho u_z \frac{\partial u_z}{\partial z} = -\frac{\partial p}{\partial z} + \rho \mu \frac{\partial^2 u_z}{\partial z^2} - \rho g \alpha \Delta T$$

$$u_z \frac{dT}{dz} = K \frac{d^2 T}{dz^2}$$

In the last term of the first equation  $g$  is the acceleration due to gravity,  $\alpha$  is the thermal expansion coefficient and  $\Delta T$  is the constant temperature difference between the plates. This term is the buoyancy force which drives the warmer, less dense, liquid upwards. In the second equation  $K$  is the thermal diffusivity (p. 190) and equals  $k/\rho C_p$  where  $k$  is the thermal conductivity and  $C_p$  is the specific heat at constant pressure.

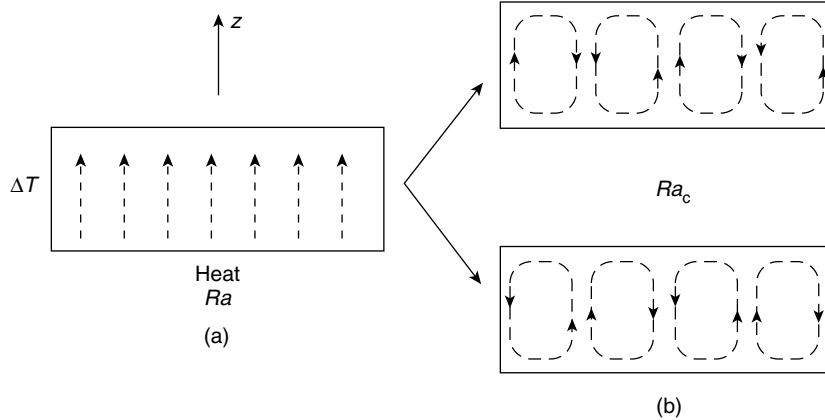


**Figure 14.38** (a) at low Rayleigh numbers  $Ra$  fluid in a Rayleigh--Bénard cell conducts heat away from the base in a symmetric fashion. At some critical value  $Ra_c$  flow symmetry is lost (b) and convective rolls develop in clockwise or anti-clockwise directions

In the first equation the buoyancy force responsible for upward motion is opposed by the viscous term. If the strength of these forces is comparable, a low pressure gradient in the fluid will keep the inertial force on the left hand side low enough for the flow to remain symmetric.

Comparable values of the buoyancy and viscous terms will give

$$\mu \frac{\partial^2 u_z}{\partial z^2} \approx g\alpha\Delta T$$

to yield some characteristic velocity

$$U \sim \frac{g\alpha\Delta TL^2}{\mu} \tag{14.1}$$

where  $L$ , a characteristic length, is usually the depth of the liquid.

The second equation determines the temperature distribution and the ratio

$$\frac{u_z dT/dz}{K d^2 T/dz^2} \sim \frac{UL}{K} \tag{14.2}$$

tells us that for  $K$  large enough the thermal conductivity will distribute the heat rapidly enough for the symmetric conduction process to prevail. Combining (14.1) and (14.2) using the common factor  $U$  gives the Rayleigh number

$$Ra = \frac{g\alpha\Delta TL^3}{\mu K}$$

When the Rayleigh number is small enough,  $\mu$  and  $K$  govern the conduction process. At some critical Rayleigh number  $Ra_c$  convective fluid motion driven by  $\Delta T$  replaces pure

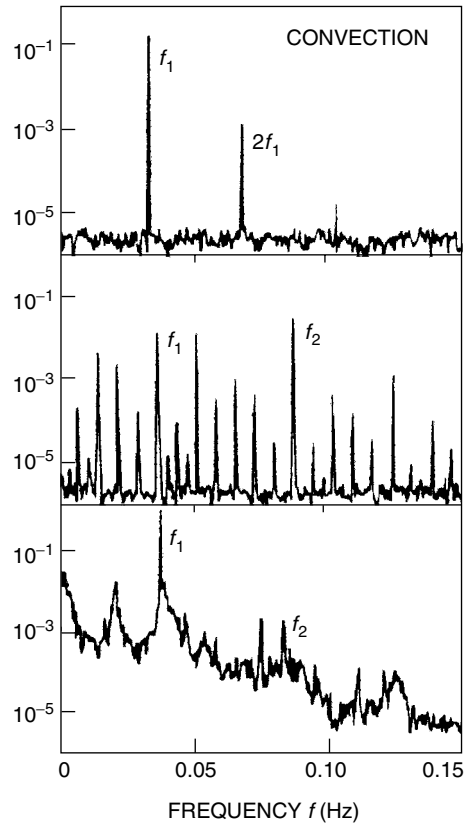


**Figure 14.39** The development of frequencies in the velocity flow spectrum at the critical Rayleigh number  $Ra_c$  with the onset of noise as chaos sets in (bottom figure). Reproduced by permission of the American Institute of Physics from Swinney and Gollub (1978)

heat conduction, instabilities develop and the flow becomes asymmetric. At the critical value  $Ra_c$  convective rolls in the right or left handed direction begin to show, with a single frequency and its harmonics appearing in the velocity flow spectrum. Increasing  $Ra$  beyond  $Ra_c$  introduces further frequency components which are followed by the onset of noise as chaos sets in (Figure 14.39).

#### *The Strange Attractor of Lorenz*

Lorenz (1963) used the Rayleigh–Bénard process as the basis of his model of atmospheric convection in assessing the possibility of long range weather forecasting. The physical model is so restricted that it yields only the most rudimentary information about weather patterns, enough however to show that long range forecasting is not feasible because phase trajectories starting from almost identical positions diverge after a relatively short time.

The two-dimensional convection rolls which appear in the rectangular cross section of Figure (14.38b) when  $Ra > Ra_c$  can be described by two velocity components together

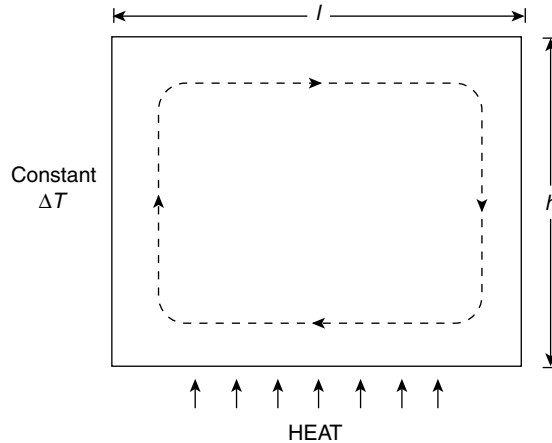


**Figure 14.40** The first mode  $X(t)$  in the Lorenz equations gives a single convective roll, clockwise for  $X$  positive, anti-clockwise for  $X$  negative. Warm rising fluid in this mode indicates where  $X$  and  $Y$  have the same sign. The ratio  $h/l$  determines the geometric factor  $b$  in the Lorenz equations

with the deviation of the temperature from the linear conduction profile of low  $Ra$ . These three quantities, two of velocity and one of temperature, were expanded in two-dimensional Fourier series with terms (modes) of the form  $A_{ij}(t) \sin k_i x \sin k_j z$  (p. 248) where the time dependence now appears in the amplitude coefficient. These expansions were used in the hydrodynamic equations of the last section to produce an infinite set of ordinary differential equations, but Lorenz reduced this number to three by considering only the first three modes of the Fourier expansion.

The first mode  $X(t)$  determined by the velocity components gives a single convective roll filling the rectangular cell (Figure 14.40). The second mode  $Y(t)$  describes the temperature differences between ascending and descending currents in the convective roll and the third mode  $Z(t)$  represents the departure from linearity of the vertical temperature profile.

Each mode is a phase space coordinate and the modes  $XYZ$  represent the physical state of the system at a given time.

The Lorenz equations take the form

$$\begin{aligned} \dot{X} &= \sigma(Y - X) \\ \dot{Y} &= rX - Y - XZ \\ \dot{Z} &= XY - bZ \end{aligned}$$

where  $\sigma$  is the ratio of the fluid viscosity to its thermal conductivity,  $r$  is the ratio  $Ra/Ra_c$  and  $b$  is a geometric factor governed by the ratio  $h/l$  (height/length) of the cell in Figure 14.40. Lorenz took  $\sigma = 10$  (the approximate value for water) and  $b = 8/3$ .

To show that the volume of phase space containing the trajectories decreased with time, Lorenz used a transport theorem of fluid dynamics relating the space rate of change of vectors describing a flow integrated over a volume  $V$  to the time rate of change of the same

volume. The vector in phase space may be written as  $F(\dot{X}, \dot{Y}, \dot{Z})$  to give

$$\frac{d}{dt} V(t) = \int_V \operatorname{div} F \, dV$$

Div  $F$  from p. 203 is given by

$$\frac{\partial \dot{X}}{\partial X} + \frac{\partial \dot{Y}}{\partial Y} + \frac{\partial \dot{Z}}{\partial Z}$$

with a value of  $-(\sigma + b + 1) = -13.67$  in Lorenz's equations, so  $dV(t)/dt$  is negative.

This reduction in phase space volume indicates that the trajectories will eventually be confined to some limiting manifold.

The overall behaviour of the system can be conveniently divided into various ranges of the value of  $r = Ra/Ra_c$ .

When

$$\dot{X} = \dot{Y} = \dot{Z} = 0$$

there are three solutions to the Lorenz equations. These are

- (1)  $X = Y = Z = 0$
- (2)  $X = Y = +[b(r - 1)]^{1/2} : Z = (r - 1)$
- (3)  $X = Y = -[b(r - 1)]^{1/2} : Z = (r - 1)$

When  $r < 1$  solution (1) corresponds to a steady process of pure conduction with no convection, typical behaviour for small  $\Delta T$ . Solutions (2) and (3) correspond to states of steady convection which exist only when  $r > 1$ .

If there is now a small perturbation from the condition  $\dot{X} = \dot{Y} = \dot{Z} = 0$  the behaviour of (1) remains stable as pure conduction for  $r < 1$ , trajectories moving to the origin  $X = Y = Z = 0$  as a point attractor. As  $r$  increases beyond unity, steady convection will give way to the right and left handed convective rolls of solutions (2) and (3) which now correspond to separate stable attractors each with its own basin of attraction and set of spiralling trajectories.

At  $r \approx 13.9$  the separation between the basins of attraction is lost and trajectories move between (2) and (3) before settling on one or the other. At  $r \approx 24.7$  (2) and (3) lose their stability as limit cycles and beyond this value of  $r$  the trajectories form two connecting bands, one centred on (2), the other on (3). (2) and (3) are now chaotic attractors with trajectories orbiting aperiodically around one before switching to the other.

### Problem 14.1

If the period of a pendulum with large amplitude oscillations is given by

$$T = T_0 \left( 1 + \frac{1}{4} \sin^2 \frac{\theta_0}{2} \right)$$

where  $T_0$  is the period for small amplitude oscillations and  $\theta_0$  is the oscillation amplitude, show that for  $\theta_0$  not exceeding  $30^\circ$ ,  $T$  and  $T_0$  differ by only 2% and for  $\theta_0 = 90^\circ$  the difference is 12%.

**Problem 14.2**

The equation of motion of a free undamped non-linear oscillator is given by

$$m\ddot{x} = -f(x)$$

Show that for an amplitude  $x_0$  its period

$$\tau_0 = 4\sqrt{\frac{m}{2}} \int_0^{x_0} \frac{dx}{[F(x_0) - F(x)]^{1/2}}, \quad \text{where } F(x_0) = \int_0^{x_0} f(x) dx$$

**Problem 14.3**

The equation of motion of a forced undamped non-linear oscillator of unit mass is given by

$$\ddot{x} = s(x) = F_0 \cos \omega t$$

Writing  $s(x) = s_1x + s_3x^3$ , where  $s_1$  and  $s_3$  are constant, choose the variable  $\omega t = \phi$ , and for  $s_3 \ll s_1$  assume a solution

$$x = \sum_{n=1}^{\infty} \left( a_n \cos \frac{n}{3} \phi + b_n \sin \frac{n}{3} \phi \right)$$

to show that all the sine terms and the even numbered cosine terms are zero, leaving the fundamental frequency term and its third harmonic as the significant terms in the solution.

**Problem 14.4**

If the mutual interionic potential in a crystal is given by

$$V = -V_0 \left[ 2 \left( \frac{r_0}{r} \right)^6 - \left( \frac{r_0}{r} \right)^{12} \right]$$

where  $r_0$  is the equilibrium value of the ion separation  $r$ , show by expanding  $V$  about  $V_0$  that the ions have small harmonic oscillations at a frequency given by  $\omega^2 \approx 72 V_0 / mr_0^2$ , where  $m$  is the reduced mass.

**Problem 14.5**

The potential energy of an oscillator is given by

$$V(x) = \frac{1}{2}kx^2 - \frac{1}{3}ax^3$$

where  $a$  is positive and  $\ll k$ .

Assume a solution  $x = A \cos \omega t + B \sin 2\omega t + x_1$  to show that this is a good approximation at  $\omega_0^2 = \omega^2 = k/m$  if  $x_1 = \alpha A^2 / 2\omega_0^2$  and  $B = -\alpha A^2 / 6\omega_0^2$ , where  $\alpha = a/m$ .

**Problem 14.6**

Prove that when  $\lambda > 0.75$  in Figure 14.11 then the slopes of  $f^2(x)$  at  $x_1^*$  and  $x_2^*$  are the same.

**Problem 14.7**

Use the arguments in the paragraph on the Cantor set (p. 495) to show that the Koch snowflake has a fractal dimension of 1.2618.

---

**Recommended Further Reading**

*Non-linear Dynamics and Chaos* by Thompson, J. M. T. and Stewart, H. B., Wiley, New York (1986).

**References**

- Feigenbaum, M. J. (1978), *Physica*, **7D**, 16.  
 Feigenbaum, M. J. (1979), *Phys. Lett.*, **74A**, 375.  
 Li, T. Y. and Yorke, J. A. (1975), *Am. Math. Monthly*, **82**, 985.  
 Lorenz, E. N. (1963), *J. Atmos. Sci.*, **20**, 130.  
 May, R. M. (1976), *Nature*, **261**, 459.  
 Metropolis, N., Stein, M. L. and Stein, P. R. (1973), *J. Combin. Theory, A*, **15**, 25.  
 Smale, S. (1963), *Differential and Combinatorial Topology* (ed. S. Cairns), Princeton University Press, Princeton, NJ.  
 Swinney, H. L. and Gollub, J. P. (1978), *Physics Today*, August, 41.  
 Tabor, M. (1989), *Chaos and Integrability in Non-linear Dynamics*, Wiley, New York.  
 Taylor, G. I. (1923), *Phil. Trans. Roy. Soc. (London), A*, **223**, 289.  
 Testa, J., Perez, J. and Jeffries, C. (1982), *Phys. Rev. Lett.*, **48**, 714.  
 Thompson, J. M. T. and Stewart, H. B. (1986), *Non-linear Dynamics and Chaos*, Wiley, New York.  
 Ueda Y. (1980) *New Approaches to Non-linear Dynamics* (ed. P. J. Holmes), S. I. A. M., Philadelphia, p. 311.  
 Van der Pol, B. (1926), *Phil. Mag.*, (7)2, 978.  
 Van der Pol, B. and Van der Mark, J. (1927), *Nature*, **120**, 363.